Shallow aquifers without Dupuit hypothesis

Christophe Bourel

Shallow aquifers without Dupuit hypothesis

Christophe Bourel[1]

[1]Univ. Littoral Côte d'Opale, LMPA, F- 62228 Calais, France

Abstract

In this paper, we present a new model as an alternative to the classical 3d-Richards model for the description of water flow in shallow aquifers. The new model is designed to meet three objectives. First, it provides a good approximation to the Richards model over a wide range of time scales. More specifically we show that both models characterize a flow with the same dominant components when the ratio of the horizontal length to the depth of the aquifer is small. Second, the new model accurately follows the velocity field. In particular, it is not based on the Dupuit hypothesis, which can be naturally considered in the context of shallow aquifers. The model can be used in the presence of wells and in aquifers with variable bedrock. We illustrate this effectiveness with numerical simulations in a not particularly shallow geometry and in the presence of sources (pumping and injection). Third, the new model allows for a numerical treatment that reduces the high computational cost associated with the Richards model. We present an efficient numerical scheme that exploits a formulation of the model as the coupling of several 1d-vertical Richards problems with a 2d-elliptic one.

Keywords. *Fluid flow modeling; Shallow aquifer; Asymptotic analysis; Richards equations; Numerical simulations; Saturated and unsaturated porous media.*

CONTENTS

1 Introduction **3**

2 Presentation of the Fast-Slow model **7**
2.1 Geometry, physical parameters and 3d-Richards problem 7
2.2 The new model that couples fast and slow flow components 9

3 Asymptotic results **11**
3.1 Dimensionless form of the 3d-Richards and *Fast-Slow* models 11
3.2 Effective problems 13
3.3 Main convergence result and dominant behaviors 15

4 Comments and general properties of the Fast-Slow model **16**
4.1 Mass conservation 16
4.2 The 3d-Richards model and the *Fast-Slow* model are not so different 17
4.3 Velocity profiles and averaged hydraulic head 17
4.4 The *Fast-Slow* model as a 1d-2d coupling model 21
4.5 Possible variants of the *Fast-Slow* model 22

5 Numerical simulations **24**
5.1 Description of the experiment 24
5.2 Reference flow characterized by 3d-Richards model 25
5.3 Velocities and water table comparison 27

6 Numerical scheme **30**
6.1 Fully implicit time scheme 30
6.2 Picard fixed-point algorithm 31

Appendix **32**
A.1 Precise definition of the data used in the numerical simulations 32
A.2 Proof of the main result for the 3d-Richards model 33
A.3 Proof of the main result for the *Fast-Slow* model 37

1. INTRODUCTION

The description of groundwater flow has been a crucial issue in water management for many years. It appears, for example, in the context of flood risk prevention. This is especially true in regions where the water table is not very deep, combined with a rainy climate. Here, the use of accurate models is mandatory to predict well the water table level and its temporal evolution, possibly over long periods and in wide aquifers. Another significant risk is the contamination of the water table, especially in regions where water is pumped and used for human consumption. Pollution in this context comes from the surface, for example due to the use of fertilizers on the fields (containing nitrates). Under the action of rain, pollutants may infiltrate the soil and be transported by water to the water table. In this case, a precise description of the subsurface flow is crucial, not only in the water table but also in the vadose zone of the aquifer. In these regions which are still rich in oxygen, the contaminants transported from the surface continue to undergo chemical reactions that can change their nature.

To characterize water flow in aquifers, the classical principle is to describe the two fluids present: air and water. This results in a complex coupled system made of two fluids that are assumed to be immiscible. It should be noted that the mobility of these two fluids in the porous soil are very different, with the mobility of air being significantly greater. In many practical situations, the air pressure in the subsurface is close to atmospheric pressure. The Richards hypothesis allows to simplify the system by describing only the pressure head of water. The problem is closed thanks to the explicit expression of the soil saturation and conductivity in terms of pressure head, see for example the Brooks and Corey [1] or the Van Genuchten [2] retention curves. The 3d-Richards model is then obtained and consists of a 3-dimensional, degenerative and nonlinear mass conservation equation. It is a parabolic PDE with a degeneracy in the time term that makes it elliptic in some regions of the domain. The Richards equations well describe the flow in the entire subsurface zone, from the bedrock to the soil. Their precise description of the vadose zone has made them popular and widely used in the context of hydrology, groundwater contamination, flood risk management...

Nevertheless difficulties arise in the practical use of this model. Its poor properties (nonlinearity and double degeneracy) in addition to the 3d nature of the problem make its numerical treatment extremely difficult and leading to costly and possibly non-converging simulations. In fact the 3d-Richards model is known as one of the most difficult problems to solve reliably and accurately in all hydrosciences [3].

There is a large bibliography on the numerical treatment of the full 3d-Richards equations. For example, we refer to [4, 5] for schemes based on modified Picard iterations to improve the robustness. In other directions, we can find methods based on variable switches [6], nested Newton loops [7], nonlinear preconditioning techniques [8] and parameterization approaches [9, 10]. Despite these advances, the practical resolution of the 3d-Richards equations generates difficult implementations and significant computational costs, which eventually become prohibitive in practical applications: for example, in the presence of a large geometry, heterogeneities and/or soil anisotropy.

Existing strategy for the simplification of the modeling. To reduce these practical difficulties, several simplified models are usually used. They consist of approximating the Richards flow by using models that exploit the shallowness of the aquifer. The best known are models based on the so-called Dupuit hypothesis [11]. They describe only the flow of the water table, that is, of the saturated part at the bottom of the aquifer. Given the slow flow dynamics in large and shallow aquifers, the water velocity is assumed to be horizontal, resulting in a 2D problem (see for example [12, 13]). These simplifications can be seen as the vertical integration of the original 3d-Richards equations over the water table. A weakness is the justification of this hypothesis, which is based on two main arguments:

- only specific length and timescales* can be considered
- the described flow is far from the injection and pumping zones (wells). Near these zones, the flow being not horizontal.

The first point can be a problem in the geochemical context of a water transport of contaminants infiltrating from the surface. The typical times of these types of chemical reactions can be very different (see [12] for empirical and qualitative arguments, and [14] for asymptotic calculations). The second point is also a limitation in this context, because a natural objective of the study could be the prevention of risks associated with well contamination. Another difficulty in the application of a 2d-Dupuit flow is its proper coupling with the overland flow. Some numerical attempts have been made in this direction. For example, it can be found in [15, 16] an integrated model directly coupled with the surface model.

A generalization of Dupuit's model is possible for shallow aquifers with non horizontal bedrock. We mention for example the recent works [17, 18] that propose a simplified model based on the averaging of the 3d-Richards equations over segments that are orthogonal to the bedrock. These works propose an averaging from the bedrock to the soil level and in particular is not limited to the water table (includes the vadose zone).

Another direction in the extension of Dupuit-like problems is of the coupling of the 2d simplified model for the water table (saturated) with several 1d-vertical Richards models to describe the recharge from the surface (unsaturated part). Such strategies can be relevant in the context of reactive transport, in particular to capture the infiltration process well. In fact, most of the chemical reactions involved depend on the oxygen level, which is naturally related to the depth where the reactions take place. This strategy has been used from a numerical point of view for example in [19, 20, 21, 22]. Let us also detail the work [23] which focuses on a mathematical justification of this type of Dupuit-Richards model. The justification is based on the characterization of the dominant components of the 3d-Richards flow that appear in shallow aquifers. It is shown that there are two dominant behaviors, depending on the time scale considered:

- the first is a *fast* component of the flow, associated with a short timescale. It consists of a collection of 1d-vertical Richards problems over the whole domain (saturated and unsaturated parts), parameterized by the horizontal position.

*In fact a long timescale is assumed when the aquifer is large.

- the second is a *slow* component of the flow, associated with a long timescale. It corresponds to a Dupuit-like flow in which the pressure profile is characterized by a vertically constant hydraulic head. This leads to a simplified 2d-horizontal problem.

Both of these problems are effective problems when the ratio $\varepsilon := \textit{depth/horizontal length}$ of the aquifer tends to zero. The purpose of [23] is to propose a coupled Dupuit/1d-Richards model defined on a bounded geometry (physical situation). It is then shown that this coupled model exhibits exactly the previous effective behavior in the $\varepsilon \to 0$ limit, regardless of the timescale. In fact the coupled problem of [23] can be seen as the coupling of the *fast* and *slow* behaviors described above in a geometrical way, the aquifer being divided into two parts. In the upper part the flow mimics the *fast* component, while in the lower part it mimics the slow component (Dupuit hypothesis).

Property 1.1. *The coupled model of [23] has the following advantages and disadvantages:*

1. *it approximates well the 3d-Richards model in shallow aquifers over a wide range of time scales (including short and long). In particular the dominant fast and slow behaviors are well described.*

2. *it is numerically simpler. It is indeed the coupling of independent 1d-vertical Richards problem[*] with a 2d horizontal problem. A significant reduction in computational time is observed compared to solving the full 3d Richards problem directly.*

3. *it describes well the evolution of the water table level even though the aquifer is not particularly shallow.*

4. *the approximation of the velocity field is not good. In fact it is purely vertical in the upper part of the aquifer and jumps to become purely horizontal in the lower part. This discontinuity disappears when the aquifer is very shallow, but is present in physical geometries. This can be a limitation in the context of contaminant transport.*

In this article, we extend the ideas of [23] to propose a new model that approximates the 3d-Richards one in shallow aquifers. The goal is to keep the same type of numerical enhancement while better describing the velocity field, thus avoiding the point 4 above. To this end we will drop Dupuit's hypothesis, responsible for the purely horizontal[†] velocity field.

Strategy of the new model. The new model presented in this paper is based on the *fast* and *slow* effective behaviors described above. We will refer to it in the following as the *Fast-Slow* model. It is given in the equations (2.11)–(2.16). The principle is to impose these effective behaviors not on different parts of the domain, as in [23], but on each direction[‡] of the velocity field, in the entire domain. More precisely the *Fast-Slow* model is constructed so that:

[*] can be solved in parallel.
[†] or at least along the bedrock direction
[‡] horizontal and vertical

- the *horizontal component of the velocity* mimics the *slow* effective behavior. It is associated with an auxiliary hydraulic head* with an explicit dependence on the vertical variable. One variant is to choose this hydraulic head as a constant over each vertical column (it is the slow effective behavior). The main *Fast-Slow* model relaxes this hypothesis by considering an auxiliary hydraulic head that is vertically constant only in the water table and is small in the upper part,

- the *vertical component of the velocity* mimics the *fast* effective behavior. It is associated with a pressure that solve a 1d-Richards problem on each vertical column. In addition, these vertical equations take into account the amount of water flowing horizontally into or out of each of these columns. This quantity appears as a source term in the vertical equations and is vertically constant in the lower part of the aquifer.

By construction the resulting water velocity has a vertical component with an affine profile in the water table. This affine profile is much less restrictive than the classical Dupuit assumption. This makes it possible to well take into account of the possibly non-constant bedrock and the presence of pumping wells.

Organization of the paper. The Section 2 is dedicated to the presentation of the *Fast-Slow* model. This is done in the equations (2.11)–(2.16) after having given some notations, the aquifer geometry and having recalled the classical 3d-Richards model (which plays the role of a reference model in this paper).

In Section 3 we give the main theorem of this article, Theorem 3.1. The latter concerns the asymptotic behaviors of the flow when the geometry of the aquifer is large and shallow. We first give the dimensionless versions of the 3d-Richards and *Fast-Slow* models, defined in a fixed reference geometry. They involve the small parameter ε, which represents the ratio *depth/horizontal length* of the aquifer. In fact, there are three dimensionless problems, each being associated with a different timescale among *short*, *intermediate* and *long*. We continue this section by presenting the three effective models corresponding to each particular timescale (see (3.22)–(3.26)). Then the main Theorem 3.1 states that, regardless of the timescale, the 3d-Richards model and the *Fast-Slow* model exhibit the same effective behaviors when ε tends to zero. In particular, this result justifies that the *Fast-Slow* model is an approximation of the reference 3d-Richards model.

In Section 4 we comment on the *Fast-Slow* model. We focus on the particular choices that we made that resulted in this version of the *Fast-Slow* model, which is tuned to approximate well the 3d-Richards flow even though the aquifer is not particularly shallow. We conclude this section with a discussion of possible variants of the *Fast-Slow* model.

The section 5 is dedicated to numerical simulations. We compare the 3d-Richards flow with that given by the *Fast-Slow* model on a test case with a non-constant bedrock and in the presence of sources (injection and pumping). They illustrate the comments given in section 4 and show the good agreement between the models.

In Section 6 we present the numerical scheme used to perform the simulations of Section 5. This scheme is fully implicit and exploits a formulation of the *Fast-Slow* model as the

*based on an average of the physical hydraulic head.

coupling of several 1d-vertical problems with a 2d horizontal one. A Picard fixed point strategy is used, resulting in a scheme that is fast in practice compared to solving the 3d-Richards problem directly.

The last section of this paper is the Appendix. It compiles the formal proof of the main Theorem (3.1), a practical calculation used in the numerical scheme, and the precise definition of the physical parameters used in the numerical simulations of Section 5.

2. Presentation of the Fast-Slow model

This section is devoted to the description of the new *Fast-Slow* model which aims to describe the flow in shallow aquifers. First, we give some notations, specify the geometry and recall the 3d-Richards problem.

2.1. Geometry, physical parameters and 3d-Richards problem

Geometry. The aquifer occupies the 3d domain $\Omega \subset \mathbb{R}^3$. We assume that it has a cylindrical shape in the vertical direction. More precisely we consider $\Omega_{2d} \subset \mathbb{R}^2$ to be a bounded domain and two functions h_{bot} and h_{soil} defined from Ω_{2d} to $\mathbb{R}$ and satisfying

$$h_{\text{soil}}(\boldsymbol{x}) > h_{\text{bot}}(\boldsymbol{x}), \qquad \forall \boldsymbol{x} = (x_1, x_2) \in \Omega_{2d}. \tag{2.1}$$

The domain Ω is then given by

$$\Omega = \big\{(\boldsymbol{x}, z) \in \Omega_{2d} \times \mathbb{R},\ z \in \big]h_{\text{bot}}(\boldsymbol{x}), h_{\text{soil}}(\boldsymbol{x})\big[\big\}. \tag{2.2}$$

In the rest of this article, we will use $\partial\Omega_{2d}$ and $\partial\Omega$ to denote the boundaries of Ω_{2d} and Ω, respectively. We will also use the letter $\boldsymbol{x}$ to denote the horizontal variables of Ω_{2d} and z for the vertical. We will also use bold letters to denote vectorial or tensor objects.

We divide the boundary $\partial\Omega$ of Ω into three parts (bottom, top and vertical) $\partial\Omega = \Gamma_{\text{bot}} \sqcup \Gamma_{\text{soil}} \sqcup \Gamma_{\text{ver}}$ with

$$\Gamma_{\text{bot}} := \big\{(\boldsymbol{x}, z) \in \Omega,\ z = h_{\text{bot}}(\boldsymbol{x})\big\}, \quad \Gamma_{\text{soil}} := \big\{(\boldsymbol{x}, z) \in \Omega,\ z = h_{\text{soil}}(\boldsymbol{x})\big\},$$
$$\Gamma_{\text{ver}} := \big\{(\boldsymbol{x}, z) \in \Omega,\ \boldsymbol{x} \in \partial\Omega_{2d}\big\}.$$

Physical parameters. The soil transmission properties are characterized by the conductivity tensor $\boldsymbol{K}(\boldsymbol{x}, z)$ and by the porosity function $\phi = \phi(\boldsymbol{x}, z) \in (0, 1)$. On the other hand the water is assumed to be incompressible and we denote its density by $\rho \in \mathbb{R}_+^*$. The conductivity tensor $\boldsymbol{K}(\boldsymbol{x}, z)$ is a 3×3 symmetric positive definite tensor which describes the conductivity of the *saturated* soil at the position $(\boldsymbol{x}, z) \in \Omega$. Its components are the functions $\boldsymbol{K}_{xx}$, K_{zz} and $\boldsymbol{K}_{xz}$, defined in Ω and valued in $\mathscr{M}_{22}(\mathbb{R})$, $\mathbb{R}^*$ and $\mathscr{M}_{21}(\mathbb{R})$ respectively, such that

$$\boldsymbol{K} = \begin{pmatrix} \boldsymbol{K}_{xx} & \boldsymbol{K}_{xz} \\ \boldsymbol{K}_{xz}^T & K_{zz} \end{pmatrix}. \tag{2.3}$$

Three-dimensional Richards problem. The aim of this paper is to propose a new model for the description of water flow in shallow aquifers. In particular we aim to derive alternatives to the classical 3d Richards equation that exploit the shallow nature of the geometry. The 3d Richards problem then plays the role of a reference model that we want to approximate in a precise and numerically efficient way.

Let us first recall this classical model and introduce some notations. We are interested in describing the flow of two immiscible fluids in the porous medium filling the domain Ω. These fluids are air and water and we denote their pressures by P_a and P respectively (in the porous medium). The first assumption in the Richards model is that the air pressure in the subsurface is equal to the atmospheric pressure, so it is not an unknown in the problem. Furthermore, the saturation s and the relative conductivity k_r of the soil are assumed to be given as functions of the fluid pressure P. They are denoted by $s = s(P)$ and $k_r = k_r(P)$ respectively. There are many models for s and k_r. The most classical example for an air-water system is the model of Brooks and Corey [1]. It is given by

$$s(P) = \begin{cases} (P_{\text{sat}}/P)^{\lambda} & \text{if } P < P_{\text{sat}} \\ 1 & \text{if } P \geq P_{\text{sat}} \end{cases}, \qquad k_r(P) = \begin{cases} (P_{\text{sat}}/P)^{\gamma} & \text{if } P < P_{\text{sat}} \\ 1 & \text{if } P \geq P_{\text{sat}} \end{cases}, \tag{2.4}$$

where $\lambda > 0$, $\gamma = 2 + 3\lambda$ and $P_{\text{sat}} < 0$. We use this particular model in the Section 5 (Numerical simulations) below. In the rest of the article we do not specify any particular choice for s and k_r. We just assume that it holds

$$s(P) = 1 \iff P \geq P_{\text{sat}} \qquad \text{and} \qquad k_r(P) = 1 \iff P \geq P_{\text{sat}}. \tag{2.5}$$

for a fixed real number P_{sat}. In particular, water pressure is greater than bubbling pressure P_{sat} if and only if the soil is fully saturated.

The water flow is then characterized by the water pressure P and the water velocity $\boldsymbol{v}$, solving the 3d Richards problem:

$$\begin{cases} \phi \dfrac{\partial s(P)}{\partial t} + \operatorname{div}(\boldsymbol{v}) = f & \text{in }]0,T[\times\Omega \\ \boldsymbol{v} = -k_r(P)\,\boldsymbol{K}\left(\dfrac{1}{\rho g}\nabla P + \boldsymbol{e}_3\right) & \text{in }]0,T[\times\Omega \end{cases} \tag{2.6}$$

where g is the gravity constant and $\boldsymbol{e}_3$ is the unitary vertical vector pointing upward. The function $f : \Omega \mapsto \mathbb{R}$ is a bulk source term and can be associated with a pumping or injection. The first equation describes the mass conservation of a constant-density fluid in the case of an incompressible soil. The second equation is Darcy's law associated with the nonlinear anisotropic conductivity $k_r(P)\,\boldsymbol{K}$.

The problem is completed with an initial condition and boundary conditions on $\partial\Omega$. We set

$$\begin{cases} \alpha P + \beta\, \boldsymbol{v}\cdot\boldsymbol{n} = f^{\text{soil}} & \text{on }]0,T[\times\Gamma_{\text{soil}} \\ \boldsymbol{v}\cdot\boldsymbol{n} = f^{\text{bot}} & \text{on }]0,T[\times\Gamma_{\text{bot}} \\ \boldsymbol{v}\cdot\boldsymbol{n} = 0 & \text{on }]0,T[\times\Gamma_{\text{ver}} \\ P(0,\boldsymbol{x},z) = P_{\text{init}}(x,z) & \text{on } \Omega \end{cases} \tag{2.7}$$

The boundary condition $\boldsymbol{v}\cdot\boldsymbol{n}=0$ on Γ_{ver} corresponds to the impermeable layer on the vertical walls of the domain. This is chosen for the sake of simplicity. At the lower boundary Γ_{bot} we consider a non homogeneous Neumann condition. In particular we allow some leakage or injection of water at the bottom of the aquifer of amplitude given by $f^{\text{bot}}:\Gamma_{\text{bot}}\to\mathbb{R}$. Of course the choice $f^{\text{bot}}=0$ characterizes an impermeable bedrock at the bottom of the aquifer.

On the other hand, we choose a general Robin condition on Γ_{soil}. It is associated with given $(\alpha,\beta)\in(\mathbb{R}^+)^2\setminus\{(0,0)\}$ and $f^{\text{soil}}:\Gamma_{\text{soil}}\to\mathbb{R}$. For example, in the presence of a river or a lake at the soil surface, assuming $\beta=0$ ensures that the pressure head of the groundwater corresponds to the depth of the overland basin. The Neumann setting $\alpha=0$ could correspond to infiltration owing to rain or irrigation.

Notations. We introduce the notations $\nabla_x=(\partial_{x_1},\partial_{x_2},0)^T$ for the horizontal gradient and $\text{div}_x(\boldsymbol{v})=\nabla_x\cdot\boldsymbol{v}=\partial_{x_1}v_1+\partial_{x_2}v_2$ for the horizontal divergence of any 3d-vector field $\boldsymbol{v}:\mathbb{R}^3\mapsto\mathbb{R}^3$.

We consider the 2×2 matrix $\boldsymbol{S}:=\boldsymbol{K}_{xx}-\frac{1}{K_{zz}}\boldsymbol{K}_{xz}\boldsymbol{K}_{zx}$ being the Schur complement of the block K_{zz} in the tensor $\boldsymbol{K}$. Furthermore, we introduce the 3×3 matrix (depending on $(\boldsymbol{x},z)$)

$$\boldsymbol{M}=\begin{pmatrix}\boldsymbol{S}&0\\0&0\end{pmatrix}. \tag{2.8}$$

We also introduce the following averaged conductivity tensors $(\tilde{\boldsymbol{K}}(\tilde{H}),\tilde{\boldsymbol{A}}(\tilde{H}))\in\mathscr{M}_{33}(\mathbb{R})$ defined for any function $\tilde{H}:\Omega_{2d}\mapsto\mathbb{R}$ by

$$\tilde{\boldsymbol{K}}(\tilde{H})=\int_{h_{\text{bot}}}^{h_{\text{soil}}}k_r\big(\rho g(\tilde{H}-z)\big)\,\boldsymbol{M}\,dz. \tag{2.9}$$

and for $\tilde{k}_r(\tilde{H}):=\int_{h_{\text{bot}}}^{h_{\text{soil}}}k_r\big(\rho g(\tilde{H}-z)\big)\,dz$, we define

$$\tilde{\boldsymbol{A}}(\tilde{H})=\frac{\tilde{\boldsymbol{K}}(\tilde{H})}{\tilde{k}_r(\tilde{H})}. \tag{2.10}$$

2.2. The new model that couples fast and slow flow components

Governing equations. The new model consists of the equations (2.11)–(2.16) below which couple the unknowns P, $\boldsymbol{v}$, $\tilde{H}$, and l. As in the 3d-Richards problem (2.6), P represents the fluid pressure and $\boldsymbol{v}$ the fluid velocity. The main principle of this model is to couple two types of flows: a *fast* component of the flow (of velocity $\boldsymbol{u}$) and a *slow* one (of velocity $\boldsymbol{w}$). We then call it in the next: *Fast-Slow* model. It consists of finding P, $\boldsymbol{v}$, $\tilde{H}$ and l such that

- The following Richards-type problem holds

$$\begin{cases}\phi\dfrac{\partial s(P)}{\partial t}+\text{div}(\boldsymbol{v})=f & \text{in }]0,T[\times\Omega\\ \alpha P+\beta\,\boldsymbol{v}\cdot\boldsymbol{n}=f_{\text{soil}} & \text{in }]0,T[\times\Gamma_{\text{soil}}\\ \boldsymbol{v}\cdot\boldsymbol{n}=f_{\text{bot}} & \text{in }]0,T[\times\Gamma_{\text{bot}}\\ \boldsymbol{v}\cdot\boldsymbol{n}=0 & \text{in }]0,T[\times\Gamma_{\text{ver}}\\ P(0,\boldsymbol{x},z)=P_{\text{init}}(\boldsymbol{x},z) & \text{for }(\boldsymbol{x},z)\in\Omega\end{cases} \tag{2.11}$$

- The lowest isolevel $P = P_{\text{sat}}$ is

$$l(t,\boldsymbol{x}) := \inf\Big\{z \in [h_{\text{bot}}(\boldsymbol{x}), h_{\text{soil}}(\boldsymbol{x})],\ P(t,\boldsymbol{x},z) \le P_{\text{sat}}\Big\}. \tag{2.12}$$

  with the convention $l(t,\boldsymbol{x}) := h_{\text{bot}}(\boldsymbol{x})$ if $P(t,\boldsymbol{x},z) > P_{\text{sat}}$ for all $z \in [h_{\text{bot}}(\boldsymbol{x}), h_{\text{soil}}(\boldsymbol{x})]$.

- The auxiliary pressure Q is given by

$$Q(t,\boldsymbol{x},z) := P_l(t,\boldsymbol{x}) + \rho g(l(t,\boldsymbol{x}) - z), \tag{2.13}$$

  with $P_l(t,\boldsymbol{x}) := P(t,\boldsymbol{x},l(t,\boldsymbol{x}))$ for all $(t,\boldsymbol{x},z) \in [0,T] \times \Omega$.

- The averaged hydraulic head is

$$\tilde{H}(t,\boldsymbol{x}) = \fint_{h_{\text{bot}}}^{l} \Big(\frac{P(t,\boldsymbol{x},z)}{\rho g} + z\Big)\, dz \qquad \text{for } (t,\boldsymbol{x}) \in [0,T[\times\Omega_{2d}. \tag{2.14}$$

  where $\fint$ is the averaged integral and with the convention $\tilde{H}(t,\boldsymbol{x}) = P_{h_{\text{bot}}}(t,\boldsymbol{x})/(\rho g) + h_{\text{bot}}(\boldsymbol{x})$ if $l(t,\boldsymbol{x}) = h_{\text{bot}}(\boldsymbol{x})$.

- The water velocity $\boldsymbol{v}$ is divided into two parts as

$$\boldsymbol{v} = \boldsymbol{u} + \boldsymbol{w} \quad \text{in } \Omega, \tag{2.15}$$

  and the auxiliary velocities (fast and slow components) are given in $]0,T[\times\Omega$ by

$$\boldsymbol{u} = -k_r(P)\, K_{zz}\Big(\frac{1}{\rho g}\frac{\partial P}{\partial z} + 1\Big)\boldsymbol{e}_3, \quad \boldsymbol{w} = -k_r(Q)\, \tilde{\boldsymbol{A}}(\tilde{H})\nabla_x \tilde{H}. \tag{2.16}$$

Property 2.1. *The model* (2.11)–(2.16) *is designed to meet the following three criteria:*

1. *to be a good approximation of the 3d-Richards model for describing the flow in shallow aquifers, over a wide range of time scales,*
2. *to be a good approximation of the 3d-Richards model even for aquifers that are not particularly shallow,*
3. *to be easier to approximate numerically than the 3d-Richards problem, in particular to allow a significant reduction in computational time.*

The justification of the claim 1 is done in Section 3 by using formal asymptotic arguments. The second property is verified and quantified numerically in Section 5. We consider a situation of an non constant bedrock, in the presence of pumping and injection. Good results are obtained even for a *ratio* of order $\mathcal{O}(1/6)$. The third property is not clear at this point. Indeed, the *Fast-Slow* model (2.11)–(2.16) is a 3d problem like the original 3d Richards one, and no immediate simplification is observed. We discuss this point in Subsection 4.4 and Section 6.

3. ASYMPTOTIC RESULTS

This section is devoted to the comparison of the 3d-Richards model (2.6) and of the *Fast-Slow* model (2.11)–(2.16) by using formal asymptotic analysis arguments. More precisely we introduce the *ratio* ε between the characteristic depth and the length of the shallow aquifer. The strategy is to scale both problems and go to the limit when $\varepsilon \to 0$ to obtain effective problems (for different time scales). Finally, we conclude because the effective problems from the 3d-Richards model and from the *Fast-Slow* model are the same, regardless of the time scale. This result is stated in Theorem 3.1 and its proof is postponed to the Appendix for ease of the presentation.

We note that the same strategy was used in the previous work [23]. In the latter the 3d-Richards model was compared with models coupling 1d-vertical Richards equations in the upper part of the aquifer with a 2d Dupuit-like problem in the lower part. Many notations are reused in the following. Moreover, in this study we consider a more general situation because the sources f, f^{soil} and f^{bot} are not assumed to be vanishing.

3.1. Dimensionless form of the 3d-Richards and *Fast-Slow* models

We use the same kind of notation as those in [23]. We introduce the dimensionless domains $\overline{\Omega} \subset \mathbb{R}^3$, $\overline{\Omega_{2d}} \subset \mathbb{R}^2$ and a dimensionless number $\overline{T} > 0$. We define the reference space-time geometry by

$$\overline{\Omega} = \left\{(\overline{\boldsymbol{x}}, \overline{z}) \in \overline{\Omega_{2d}} \times \mathbb{R},\ \overline{z} \in \left]\overline{h}_{\text{bot}}(\overline{\boldsymbol{x}}), \overline{h}_{\text{soil}}(\overline{\boldsymbol{x}})\right[\right\},$$

for given functions $\overline{h}_{\text{soil}}$ and $\overline{h}_{\text{bot}}$ defined from $\overline{\Omega_{2d}}$ to $\mathbb{R}$. We divide the boundary $\partial\overline{\Omega}$ into the three parts $\overline{\Gamma}_{\text{bot}} := \{(\overline{\boldsymbol{x}}, \overline{z}) \in \overline{\Omega},\ \overline{z} = \overline{h}_{\text{bot}}(\overline{\boldsymbol{x}})\}$, $\overline{\Gamma}_{\text{soil}} := \{(\overline{\boldsymbol{x}}, \overline{z}) \in \overline{\Omega},\ \overline{z} = \overline{h}_{\text{soil}}(\overline{\boldsymbol{x}})\}$ and $\overline{\Gamma}_{\text{ver}} := \{(\overline{\boldsymbol{x}}, \overline{z}) \in \overline{\Omega},\ \overline{\boldsymbol{x}} \in \partial\overline{\Omega_{2d}}\}$. We also introduce the positive numbers L_x, L_z, T to recover the physical variables from the dimensionless ones by

$$\boldsymbol{x} = L_x \overline{\boldsymbol{x}}, \quad z = L_z \overline{z}, \quad t = T\overline{t}/\overline{T}.$$

With these notations, the domain Ω is a dilation of the reference domain $\overline{\Omega}$ thanks to

$$\Omega_{2d} = L_x \overline{\Omega_{2d}}, \quad h_{\text{soil}}(\boldsymbol{x}) = L_z\, \overline{h}_{\text{soil}}(\overline{\boldsymbol{x}}), \quad h_{\text{bot}}(\boldsymbol{x}) = L_z\, \overline{h}_{\text{bot}}(\overline{\boldsymbol{x}}).$$

The exterior normal associated with $\partial\overline{\Omega}$ has the form

$$\overline{\boldsymbol{n}}(\overline{\boldsymbol{x}}, \overline{z}) = \begin{cases} \left(\boldsymbol{e}_3 - (L_z/L_x)\nabla_{\overline{x}}\overline{h}_{\text{soil}}(\overline{\boldsymbol{x}})\right)\left((L_z^2/L_x^2)|\nabla_{\overline{x}}\overline{h}_{\text{soil}}(\overline{\boldsymbol{x}})|^2 + 1\right)^{-1/2} & \text{on } \overline{\Gamma}_{\text{soil}} \\ \left((L_z/L_x)\nabla_{\overline{x}}\overline{h}_{\text{bot}}(\overline{\boldsymbol{x}}) - \boldsymbol{e}_3\right)\left((L_z^2/L_x^2)|\nabla_{\overline{x}}\overline{h}_{\text{bot}}(\overline{\boldsymbol{x}})|^2 + 1\right)^{-1/2} & \text{on } \overline{\Gamma}_{\text{bot}} \\ \boldsymbol{n}(\boldsymbol{x}, z) & \text{on } \overline{\Gamma}_{\text{ver}}. \end{cases}$$

In particular, the vector $\boldsymbol{n}$ in the last equation is horizontal (because $\overline{\Gamma}_{\text{ver}}$ is vertical) and does not change during the scaling.

We introduce the rescaled unknowns of the 3d-Richards and *Fast-Slow* models

$$L_z\overline{P}(\overline{t}, \overline{\boldsymbol{x}}, \overline{z}) = P(t, \boldsymbol{x}, z), \quad \overline{\boldsymbol{v}}(\overline{t}, \overline{\boldsymbol{x}}, \overline{z}) = v(t, \boldsymbol{x}, z), \quad \overline{\boldsymbol{u}}(\overline{t}, \overline{\boldsymbol{x}}, \overline{z}) = u(t, \boldsymbol{x}, z), \quad \overline{\boldsymbol{w}}(\overline{t}, \overline{\boldsymbol{x}}, \overline{z}) = w(t, \boldsymbol{x}, z),$$
$$L_z\overline{H}(\overline{t}, \overline{\boldsymbol{x}}) = \tilde{H}(t, \boldsymbol{x}),$$

On the other hand, the saturation and the relative conductivity functions are not affected by the change of variable:

$$s(L_z\overline{P}) = s(P), \qquad k_r(L_z\overline{P}) = k_r(P). \tag{3.1}$$

The rescaled conductivity tensors and source terms are chosen as

$$\overline{\boldsymbol{K}}(\overline{\boldsymbol{x}},\overline{z}) = \boldsymbol{K}(\boldsymbol{x},z), \quad \overline{\boldsymbol{M}}(\overline{\boldsymbol{x}},\overline{z}) = \boldsymbol{M}(\boldsymbol{x},z), \tag{3.2}$$

$$\overline{\boldsymbol{K}}(\overline{H})(\overline{t},\overline{\boldsymbol{x}}) = L_z \int_{\overline{h}_{\mathrm{bot}}(\overline{\boldsymbol{x}})}^{\overline{h}_{\mathrm{soil}}(\overline{\boldsymbol{x}})} k_r\big(\rho g(\overline{H}(\overline{t},\overline{\boldsymbol{x}}) - \overline{z})\big)\overline{\boldsymbol{M}}\, d\overline{z}, \tag{3.3}$$

$$\overline{f}(\overline{t},\overline{\boldsymbol{x}}) = f(t,\boldsymbol{x}), \qquad \overline{f}^{\mathrm{soil}}(\overline{t},\overline{\boldsymbol{x}}) = f^{\mathrm{soil}}(t,\boldsymbol{x}), \qquad \overline{f}^{\mathrm{bot}}(\overline{t},\overline{\boldsymbol{x}}) = f^{\mathrm{bot}}(t,\boldsymbol{x}).$$

Finally, the initial pressure is $\overline{P_{\mathrm{init}}}(\overline{x},\overline{z}) := P_{\mathrm{init}}(x,z)$.

Dimensionless Richards problem. Taking into account on the previous quantities, Equations (2.6) and (2.7) yield

$$\frac{\overline{T}}{T}\phi\frac{\partial s(L_z\overline{P})}{\partial\overline{t}} + \frac{1}{L_x}\operatorname{div}_{\overline{\boldsymbol{x}}}(\overline{\boldsymbol{v}}) + \frac{1}{L_z}\frac{\partial\overline{\boldsymbol{v}}}{\partial\overline{z}} = \overline{f} \quad \text{in }]0,\overline{T}[\times\overline{\Omega}, \tag{3.4}$$

$$\overline{\boldsymbol{v}} = -k_r(L_z\overline{P})\,\overline{\boldsymbol{K}}\Big(\frac{L_z}{L_x}\frac{1}{\rho g}\nabla_{\overline{x}}\overline{P} + \Big(\frac{1}{\rho g}\frac{\partial\overline{P}}{\partial\overline{z}} + 1\Big)\boldsymbol{e}_3\Big) \quad \text{in }]0,\overline{T}[\times\overline{\Omega}, \tag{3.5}$$

$$\overline{\boldsymbol{v}}\cdot\Big(\frac{L_z}{L_x}\nabla_{\overline{x}}\overline{h}_{\mathrm{bot}} - \boldsymbol{e}_3\Big) = \overline{f}^{\mathrm{bot}}\Big(\frac{L_z^2}{L_x^2}\|\nabla_{\overline{x}}\overline{h}_{\mathrm{soil}}\|^2 + 1\Big)^{1/2} \quad \text{on }]0,\overline{T}[\times\overline{\Gamma}_{\mathrm{bot}}, \tag{3.6}$$

$$\alpha\, L_z\overline{P}\Big(\frac{L_z^2}{L_x^2}\|\nabla_{\overline{x}}\overline{h}_{\mathrm{soil}}\|^2+1\Big)^{1/2} + \beta\,\overline{\boldsymbol{v}}\cdot\Big(\boldsymbol{e}_3 - \frac{L_z}{L_x}\nabla_{\overline{x}}\overline{h}_{\mathrm{soil}}\Big) = \overline{f}^{\mathrm{soil}}\Big(\frac{L_z^2}{L_x^2}\|\nabla_{\overline{x}}\overline{h}_{\mathrm{soil}}\|^2+1\Big)^{1/2} \quad \text{on }]0,\overline{T}[\times\overline{\Gamma}_{\mathrm{soil}}, \tag{3.7}$$

$$\overline{\boldsymbol{v}}\cdot\overline{\boldsymbol{n}} = 0 \quad \text{on }]0,\overline{T}[\times\overline{\Gamma}_{\mathrm{ver}}. \tag{3.8}$$

$$\overline{P}(0,\overline{x},\overline{z}) = \overline{P_{\mathrm{init}}}(\overline{x},\overline{z}) \qquad \text{on } \overline{\Omega} \tag{3.9}$$

We are interested in shallow aquifers with a small vertical depth relative to the horizontal length. The quantity $L_z/L_x := \varepsilon$ is then small. We choose the scaling

$$L_z = 1 \qquad \text{and} \qquad L_x = 1/\varepsilon.$$

The mass conservation equation (3.4) depends on the choice of time scaling T and has the form

$$\frac{\overline{T}}{T}\phi\frac{\partial s(\overline{P})}{\partial\overline{t}} + \varepsilon\operatorname{div}_{\overline{\boldsymbol{x}}}(\overline{\boldsymbol{v}}) + \frac{\partial\overline{\boldsymbol{v}}\cdot\boldsymbol{e}_3}{\partial\overline{z}} = \overline{f} \qquad \text{in }]0,\overline{T}[\times\overline{\Omega}. \tag{3.10}$$

The corresponding Darcy's law (3.5) is as follows

$$\overline{\boldsymbol{v}} = -k_r(\overline{P})\,\overline{\boldsymbol{K}}\Big(\frac{\varepsilon}{\rho g}\nabla_{\overline{x}}\overline{P} + \Big(\frac{1}{\rho g}\frac{\partial\overline{P}}{\partial\overline{z}} + 1\Big)\boldsymbol{e}_3\Big) \qquad \text{in }]0,\overline{T}[\times\overline{\Omega}. \tag{3.11}$$

The boundary conditions are

$$\begin{cases} \alpha\,\overline{P}\left(\varepsilon^2\,\|\nabla_{\overline{x}}\overline{h}_{\rm soil}\|^2+1\right)^{1/2}+\beta\,\overline{\boldsymbol{v}}\cdot\left(\boldsymbol{e}_3-\varepsilon\,\nabla_{\overline{x}}\overline{h}_{\rm soil}\right)=\left(\varepsilon^2\,\|\nabla_{\overline{x}}\overline{h}_{\rm soil}\|^2+1\right)^{1/2}\overline{f}^{\rm soil} & \text{on }]0,\overline{T}[\times\overline{\Gamma}_{\rm soil},\\ \overline{\boldsymbol{v}}\cdot\overline{\boldsymbol{n}}=0 & \text{on }]0,\overline{T}[\times\overline{\Gamma}_{\rm ver},\\ \overline{\boldsymbol{v}}\cdot\left(\varepsilon\nabla_{\overline{x}}\overline{h}_{\rm bot}-\boldsymbol{e}_3\right)=\left(\varepsilon^2\,\|\nabla_{\overline{x}}\overline{h}_{\rm soil}\|^2+1\right)^{1/2}\overline{f}^{\rm bot} & \text{on }]0,\overline{T}[\times\overline{\Gamma}_{\rm bot}. \end{cases} \tag{3.12}$$

The initial pressure is given by

$$\overline{P}(0,\overline{\boldsymbol{x}},\overline{z})=\overline{P_{\rm init}}(\overline{\boldsymbol{x}},\overline{z})\qquad\text{for } (\overline{\boldsymbol{x}},\overline{z})\in\overline{\Omega}. \tag{3.13}$$

Dimensionless *Fast-Slow* model. For the same parameter $\varepsilon\ll 1$, the rescaled version of the *Fast-Slow* model (2.11)–(2.16) is given below:

The mass-conservation equation (3.10) and the boundary conditions (3.12) still hold (see Equation (2.11)). The corresponding dimensionless velocities are

$$\begin{cases} \overline{\boldsymbol{v}}=\overline{\boldsymbol{u}}+\overline{\boldsymbol{w}} & \text{in }]0,\overline{T}[\times\overline{\Omega},\\ \overline{\boldsymbol{u}}=-k_r(\overline{P})\,\overline{K}_{zz}\left(\dfrac{1}{\rho g}\dfrac{\partial\overline{P}}{\partial\overline{z}}+1\right)\boldsymbol{e}_3 & \text{in }]0,\overline{T}[\times\overline{\Omega},\\ \overline{\boldsymbol{w}}=-\varepsilon\,k_r(\overline{Q})\overline{\boldsymbol{A}}(\overline{H})\nabla_x\overline{H} & \text{in }]0,\overline{T}[\times\overline{\Omega}. \end{cases} \tag{3.14}$$

The auxiliary pressure is

$$\overline{Q}(\overline{t},\overline{\boldsymbol{x}},\overline{z})=\overline{P}_l(\overline{t},\overline{\boldsymbol{x}})+\rho g\big(\overline{l}(\overline{t},\overline{\boldsymbol{x}})-\overline{z}\big), \tag{3.15}$$

with $\overline{P}_l(\overline{t},\overline{\boldsymbol{x}})=\overline{P}(\overline{t},\overline{\boldsymbol{x}},\overline{l}(\overline{t},\overline{\boldsymbol{x}}))$. The averaged hydraulic head is

$$\overline{H}(t,\boldsymbol{x})=\fint_{\overline{h}_{\rm bot}}^{\overline{l}}\left(\frac{\overline{P}(\overline{t},\overline{\boldsymbol{x}},\overline{z})}{\rho g}+\overline{z}\right)d\overline{z}\qquad\text{in }]0,\overline{T}[\times\overline{\Omega_{2d}}. \tag{3.16}$$

The lowest isolevel $\overline{P}=P_{\rm sat}$ takes the form

$$\overline{l}(\overline{t},\overline{\boldsymbol{x}}):=\inf\left\{\overline{z}\in[\overline{h}_{\rm bot}(\overline{\boldsymbol{x}}),\overline{h}_{\rm soil}(\overline{\boldsymbol{x}})],\ \overline{P}(\overline{t},\overline{\boldsymbol{x}},\overline{z})\le P_{\rm sat}\right\}\quad\text{for } (\overline{t},\overline{\boldsymbol{x}})\in[0,\overline{T}[\times\overline{\Omega_{2d}}. \tag{3.17}$$

3.2. Effective problems

In this part we give effective problems derived from the dimensionless models above, associated with three different timescales. More precisely, we aim to describe effective flows associated with the short timescale $T=\overline{T}$, the intermediate timescale $T=\varepsilon^{-1}\overline{T}$ and the long timescale $T=\varepsilon^{-2}\overline{T}$.

Formal asymptotic expansion. For $\gamma\in\{0,1,2\}$ and $\varepsilon>0$, we denote P_ε^γ the solutions of the problem (3.10)-(3.13) or (3.10), (3.12)-(3.17) associated to the time scale $T=\varepsilon^{-\gamma}\overline{T}$. We use the same notation for the other variables $\overline{\boldsymbol{v}}_\varepsilon^\gamma$, $\overline{\boldsymbol{u}}_\varepsilon^\gamma$...

For each of these functions, we consider the following formal asymptotics,

$$\overline{P}_\varepsilon^\gamma=\overline{P}_0^\gamma+\varepsilon\,\overline{P}_1^\gamma+\varepsilon^2\,\overline{P}_2^\gamma+\ldots\qquad\overline{\boldsymbol{v}}_\varepsilon^\gamma=\overline{\boldsymbol{v}}_0^\gamma+\varepsilon\,\overline{\boldsymbol{v}}_1^\gamma+\varepsilon^2\,\overline{\boldsymbol{v}}_2^\gamma+\ldots \tag{3.18}$$

We also assume the existence of formal asymptotics for auxiliary unknowns in (2.11)–(2.16)

$$\begin{aligned} \overline{\boldsymbol{u}}^\gamma_\varepsilon &= \overline{\boldsymbol{u}}^\gamma_0 + \varepsilon\,\overline{\boldsymbol{u}}^\gamma_1 + \varepsilon^2\,\overline{\boldsymbol{u}}^\gamma_2 + \dots & \overline{\boldsymbol{w}}^\gamma_\varepsilon &= \overline{\boldsymbol{w}}^\gamma_0 + \varepsilon\,\overline{\boldsymbol{w}}^\gamma_1 + \varepsilon^2\,\overline{\boldsymbol{w}}^\gamma_2 + \dots \\ \overline{H}^\gamma_\varepsilon &= \overline{H}_0 + \varepsilon\,\overline{H}^\gamma_1 + \varepsilon^2\,\overline{H}^\gamma_2 + \dots & \overline{l}^\gamma_\varepsilon &= \overline{l}^\gamma_0 + \varepsilon\,\overline{l}^\gamma_1 + \varepsilon^2\,\overline{l}^\gamma_2 + \dots, \end{aligned} \tag{3.19}$$

and for the sources

$$\overline{f}_\varepsilon = \overline{f}_0 + \varepsilon\,\overline{f}_1 + \varepsilon^2\,\overline{f}_2 + \dots, \quad \overline{f}^{\rm soil}_\varepsilon = \overline{f}^{\rm soil}_0 + \varepsilon\,\overline{f}^{\rm soil}_1 + \dots, \quad \overline{f}^{\rm bot}_\varepsilon = \overline{f}^{\rm bot}_0 + \varepsilon\,\overline{f}^{\rm bot}_1 + \dots. \tag{3.20}$$

Moreover, as s and k_r are piecewise $\mathscr{C}^\infty$ functions, we write

$$\begin{aligned} s(\overline{P}^\gamma_\varepsilon) &= s(\overline{P}^\gamma_0) + \varepsilon(\overline{P}^\gamma_1 + \varepsilon\,\overline{P}^\gamma_2 + \dots)s'(\overline{P}^\gamma_0) + \frac{\varepsilon^2}{2}(\overline{P}^\gamma_1 + \varepsilon\,\overline{P}^\gamma_2 + \dots)^2 s''(\overline{P}^\gamma_0) + \dots \\ k_r(\overline{P}^\gamma_\varepsilon) &= k_r(\overline{P}^\gamma_0) + \varepsilon(\overline{P}^\gamma_1 + \varepsilon\,\overline{P}^\gamma_2 + \dots)k_r'(\overline{P}^\gamma_0) + \frac{\varepsilon^2}{2}(\overline{P}^\gamma_1 + \varepsilon\,\overline{P}^\gamma_2 + \dots)^2 k_r''(\overline{P}^\gamma_0) + \dots \end{aligned} \tag{3.21}$$

Effective problems at the main order. We give effective problems characterizing the 0-order term P^γ_0 in the expansion (3.18) for each case of the time scale $\gamma \in \{0,1,2\}$:

- related to the short timescale $\gamma = 0$ ($T = \overline{T}$),

$$\begin{cases} \phi\,\dfrac{\partial s(\overline{P}_0)}{\partial \overline{t}} + \dfrac{\partial \overline{v}^3_0}{\partial \overline{z}} = \overline{f}_0 & \text{in }]0,\overline{T}[\times\Omega \\ \overline{v}^3_0 = -k_r(\overline{P}_0)\,\overline{K}_{zz}\Big(\dfrac{1}{\rho g}\dfrac{\partial \overline{P}_0}{\partial \overline{z}} + 1\Big) & \text{in }]0,\overline{T}[\times\Omega \\ \alpha\,\overline{P}_0 + \beta\,\overline{v}^3_0 = \overline{f}^{\rm soil}_0 & \text{on }]0,\overline{T}[\times\overline{\Gamma}_{\rm soil} \\ \overline{v}^3_0 = \overline{f}^{\rm bot}_0 & \text{on }]0,\overline{T}[\times\overline{\Gamma}_{\rm bot} \end{cases} \tag{3.22}$$

- related to the non-short timescale $\gamma > 0$ ($T = \varepsilon^{-1}\overline{T}$ or $T = \varepsilon^{-2}\overline{T}$),

$$\begin{cases} \overline{P}_0(t,\boldsymbol{x},z) = \rho g\big(\overline{H}_0(t,\boldsymbol{x}) - \overline{z}\big) & \text{in }]0,\overline{T}[\times\overline{\Omega} \\ \overline{\boldsymbol{v}}_0 = 0 & \text{in }]0,\overline{T}[\times\overline{\Omega} \end{cases} \tag{3.23}$$

- related to the non-short timescale $\gamma > 0$ ($T = \varepsilon^{-1}\overline{T}$ or $T = \varepsilon^{-2}\overline{T}$) if $\alpha \neq 0$

$$\overline{H}_0(\overline{t},\overline{\boldsymbol{x}}) = \frac{\overline{f}^{\rm soil}_0(\overline{t},\overline{\boldsymbol{x}})}{\alpha\,\rho g} + \overline{h}_{\rm soil}(\overline{t},\overline{\boldsymbol{x}}) \qquad \text{in }]0,\overline{T}[\times\overline{\Omega_{2d}} \tag{3.24}$$

- related to the intermediate timescale $\gamma = 1$ ($T = \varepsilon^{-1}\overline{T}$) if $\alpha = 0$ (and then $\beta \neq 0$)

$$\rho g\Big(\int_{\overline{h}_{\rm bot}}^{\overline{h}_{\rm soil}} \phi\,s'(\overline{P}_0)\,dz\Big)\frac{\partial \overline{H}_0}{\partial t} = \int_{\overline{h}_{\rm bot}}^{\overline{h}_{\rm soil}} \overline{f}_1\,dz + \frac{\overline{f}^{\rm bot}_1}{\beta} - \frac{\overline{f}^{\rm soil}_1}{\beta} \qquad \text{in }]0,\overline{T}[\times\overline{\Omega_{2d}} \tag{3.25}$$

- related to the long timescale $\gamma = 2$ ($T = \varepsilon^{-2}\overline{T}$) if $\alpha = 0$ (and then $\beta \neq 0$)

$$\begin{cases} \dfrac{\partial}{\partial \overline{t}}\Big(\displaystyle\int_{\overline{h}_{\rm bot}}^{\overline{h}_{\rm soil}} \phi\, s(\overline{P}_0)\, d\overline{z}\Big) + \mathrm{div}_x(\overline{\boldsymbol{w}}) = \int_{\overline{h}_{\rm bot}}^{\overline{h}_{\rm soil}} \overline{f}_2\, dz + \dfrac{\overline{f}_2^{\rm bot}}{\beta} - \dfrac{\overline{f}_2^{\rm soil}}{\beta} & \text{in }]0,\overline{T}[\times\overline{\Omega_{2d}} \\ \overline{\boldsymbol{w}} = -\overline{\boldsymbol{K}}(\overline{H}_0)\,\nabla_x \overline{H}_0 & \text{in }]0,\overline{T}[\times\overline{\Omega_{2d}} \\ \overline{\boldsymbol{w}}\cdot\overline{\boldsymbol{n}} = 0 & \text{on }]0,\overline{T}[\times\overline{\Gamma}_{\rm ver} \end{cases} \tag{3.26}$$

Note that the function $\overline{l}$ does not appear in effective problems (3.22)-(3.26). This indicates that the choice of $\overline{l}$ has no effect on effective problems. However, this choice could play a significant role in the model (2.11)–(2.16) which is not effective as the ratio *depth/horizontal length* of the aquifer is a fixed positive number. We discuss this point in Section 4.

We also notice that almost the same effective problems (3.22)-(3.26) have already been obtained in the previous work [23] (Equations (3.22)-(3.27)). More precisely we now consider the sources $f^{\rm bot}$ and f (see equations (2.6) and (2.7)). Their contributions appear in the equations (3.22), (3.25) and (3.26).

3.3. Main convergence result and dominant behaviors

Theorem 3.1. *Let $(\overline{P}_\varepsilon^\gamma, \overline{\boldsymbol{v}}_\varepsilon^\gamma)$ be the solution of the rescaled 3d-Richards problem* (3.10)–(3.11) or *of the rescaled coupled problem* (3.10), (3.12)-(3.17) *for $T = \varepsilon^{-\gamma}\overline{T}$ and $\gamma \in \{0,1,2\}$. Assume that* (3.18)–(3.21) *hold true. The main order terms of the pressure and the velocity of the fluid are characterized by*

(i) $\overline{P}_0^0$ *satisfies* (3.22).

(ii) If the sources are such that

$$\overline{f}_0^{\rm bot} = 0 \quad \textit{and} \quad \overline{f}_0 = 0, \tag{3.27}$$

- *if $\alpha \neq 0$, $(\overline{P}_0^1, \overline{\boldsymbol{v}}_0^1)$ satisfies* (3.23) *and* (3.24),
- *if $\alpha = 0$, $(\overline{P}_0^1, \overline{\boldsymbol{v}}_0^1)$ satisfies* (3.23) *and* (3.25) *with the compatibility condition $\overline{f}_0^{\rm soil} = 0$.*

(iii) If the sources are such that

$$\overline{f}_0^{\rm bot} = \overline{f}_1^{\rm bot} = 0 \quad \textit{and} \quad \overline{f}_0 = \overline{f}_1 = 0, \tag{3.28}$$

- *if $\alpha \neq 0$, $(\overline{P}_0^2, \overline{\boldsymbol{v}}_0^2)$ satisfies* (3.23) *and* (3.24),
- *if $\alpha = 0$, $(\overline{P}_0^2, \overline{\boldsymbol{v}}_0^2)$ satisfies* (3.23) *and* (3.26) *with the compatibility condition $\overline{f}_0^{\rm soil} = \overline{f}_1^{\rm soil} = 0$.*

To simplify the presentation, we postpone the proof of this Theorem to the Appendix. Let us look at some of its implications.

This Theorem 3.1 first characterizes the dominant components of a 3d-Richards flow in the three time scale cases: short ($\gamma = 0$), intermediate ($\gamma = 1$) and long ($\gamma = 2$). We briefly describe these types of flows in the next part.

The second result given by Theorem 3.1 is that the flow described by a 3d-Richards system and that described by the *Fast-Slow* model exhibits exactly the same dominant behavior for each time-scale considered. It is in this sense that the *Fast-Slow* model approximates the 3d-Richards model. Moreover, this approximation is robust because it holds over a wide range of time scales.

Dominant behavior in shallow aquifers. We refer to [23] for more details on these kinds of dominant flows (obtained in the case of $f = f^{\text{bot}} = 0$).

In the case of short time scale, corresponding to $\overline{T} = T$, the pressure $\overline{P}_0$ solves (3.22). This is a 1d-vertical Richards problem where the horizontal variable $\overline{x} \in \overline{\Omega_{2d}}$ is only a parameter. In particular, there is no horizontal flow. One possible interpretation is that the time of the experiment is too short for the horizontal flow to be significant (relative to the large horizontal dimension of the aquifer). Then only the vertical flow appears at this scale.

For the other time scales, corresponding to $\overline{T} = \varepsilon^{-\gamma} T$ for $\gamma \in \{1,2\}$, we assume $\overline{f}_0 = 0$ and $\overline{f}_0^{\text{bot}} = 0$. The pressure $\overline{P}_0$ exhibits a vertical affine profile (3.23). In particular the associated hydraulic head is $\overline{H}_0$ and is constant in the vertical direction. This can be interpreted as follows: we are in the case where the experiment time is infinite. Then the dominant vertical flow is over and the steady state of the 1d-Richards equation is reached. This steady state corresponds exactly to the affine profile for the pressure $\overline{P}_0$ given above.

Let us consider the non-short time scale $\gamma \in \{1,2\}$ cases when $\alpha \neq 0$. Then the hydraulic head $\overline{H}_0$ (constant / z) is characterized by the boundary condition at the soil level, see Equation (3.24). The affine pressure profile (3.23) holds for $\overline{P}_0$ and the boundary condition imposes the value of $\overline{H}_0$ without leaving any degrees of freedom.

In the case of the intermediate time scale $T = \overline{T}/\varepsilon$, if $\alpha = 0$, the boundary condition at the soil level does not directly fix $\overline{H}_0$ but imposes the compatibility condition $\overline{f}^{\text{soil}} = 0$. The hydraulic head $\overline{H}_0$ is characterized by Equation (3.25). In this equation, the variable $\overline{x}$ acts only as a parameter. In a sense, this time scale is extremely long and thus the vertical flow is finished. However, it is also too short to capture the horizontal flow.

In the case of long time scale $T = \overline{T}/\gamma^2$, if $\alpha = 0$, we assume $\overline{f}_0 = \overline{f}_1 = 0$ and $\overline{f}_0^{\text{bot}} = \overline{f}_1^{\text{bot}} = 0$. The hydraulic head $\overline{H}_0$ satisfies Equation (3.26). It is a 2d mass conservation equation in the horizontal direction. It is associated with the horizontal velocity $-\overline{K}(\overline{H}_0)\nabla_x \overline{H}_0$. Note that this time scale is the one that captures a non-trivial dominant horizontal flow in shallow aquifers.

4. Comments and general properties of the Fast-Slow model

4.1. Mass conservation

The first property of the *Fast-Slow* model (2.11)–(2.16) is that it is mass conservative in the following sense.

Proposition 4.1. *Let $(P, \boldsymbol{v})$ be the solution of* (2.11)–(2.16). *Let $V(t)$ be the total volume of water in the aquifer defined by*

$$V(t) = \int_\Omega \phi\, s(P)\, d\boldsymbol{x}\, dz. \tag{4.1}$$

Then it holds

$$\frac{\partial V}{\partial t} = \int_\Omega f \, d\boldsymbol{x}\, dz - \int_{\Gamma_{\text{bot}}} f^{\text{bot}} - \int_{\Gamma_{\text{soil}}} \boldsymbol{v}\cdot\boldsymbol{n} \quad in\ [0,T]. \tag{4.2}$$

We get this result by integrating the first equation in (2.11) over Ω, by using an integration by parts and by taking into account the boundary conditions in (2.11).

This result is exactly the same as that which can be obtained for the original 3d-Richards model. It is expected, of course, since the mass conservation equation and the boundary conditions in the *Fast-Slow* model (see Equation (2.11)) are exactly the same as those in the 3d-Richards model (see the first equation in (2.6) and Equation (2.7)). In the new model, only the definition of the velocity differs from that of the 3d-Richards model.

4.2. The 3d-Richards model and the *Fast-Slow* model are not so different

As noted above, the 3d-Richards model (2.6)-(2.7) and the *Fast-Slow* model (2.11)–(2.16) are characterized by the same mass-conservation equation $\phi\frac{\partial s(P)}{\partial t} + \text{div}(\boldsymbol{v}) = f$. These problems differ only in the definition of the associated velocity.

We denote in this part $(\hat{P}, \hat{\boldsymbol{v}})$ the solution of the 3d-Richards problem (2.6)-(2.7) and $(P, \boldsymbol{v})$ the solution of the *Fast-Slow* problem (2.11)–(2.16). Keeping the notation (2.3) in mind, we split the velocity $\hat{\boldsymbol{v}}$ as $\hat{\boldsymbol{v}} = \hat{\boldsymbol{u}} + \hat{\boldsymbol{w}}$ where $(\hat{\boldsymbol{u}}, \hat{\boldsymbol{w}})$ are defined by

$$\hat{\boldsymbol{u}} = -k_r(\hat{P})\, K_{zz}\Big(\frac{1}{\rho g}\frac{\partial \hat{P}}{\partial z} + 1\Big)\boldsymbol{e}_3, \quad \hat{\boldsymbol{w}} = -k_r(\hat{P})\,\hat{\boldsymbol{L}}\Big(\frac{1}{\rho g}\nabla\hat{P} + \boldsymbol{e}_3\Big), \quad \text{with} \quad \hat{\boldsymbol{L}} = \begin{pmatrix} \boldsymbol{K}_{xx} & \boldsymbol{K}_{xz} \\ \boldsymbol{K}_{xz}^T & 0 \end{pmatrix}. \tag{4.3}$$

Note that the velocity $\hat{\boldsymbol{u}}$ above is exactly the one that appears in the effective problem (3.23); this one describes the effective flow in the case of short time scale. The $\hat{\boldsymbol{u}}$ component of the velocity then corresponds to a fast component of the flow. We keep this definition for $\boldsymbol{u}$ in the *Fast-Slow* model, see Equation (2.16). In particular $\boldsymbol{u}$ is vertical.

On the other hand the second term $\hat{\boldsymbol{w}}$ will represent a slower component of the flow. In the *Fast-Slow* model, we change its definition to simplify the model by neglecting the non-dominant components of the flow. An averaged version of $\hat{\boldsymbol{w}}$ is chosen (see Equation (2.16)). It is based on an averaged hydraulic head $\tilde{H}$, on an auxiliary pressure Q, and on an averaged version of the conductivity tensor $k_r(\hat{P})\hat{\boldsymbol{L}}$ given by $k_r(Q)\tilde{\boldsymbol{A}}$ (see (2.10)). This particular choice was made so that $\boldsymbol{w}$ fits well with effective velocity in the long time scale case (see Equation (3.26)). Note also that the shape of $\tilde{\boldsymbol{A}}$ is different from that of $\hat{\boldsymbol{L}}$. In particular $\boldsymbol{w}$ is necessarily horizontal, while $\hat{\boldsymbol{w}}$ is not.

4.3. Velocity profiles and averaged hydraulic head

The "slow" component $\boldsymbol{w}$. As mentioned above, the component $\boldsymbol{w}$ will describe the slow component of the flow. It is defined in (2.16) while the function $\tilde{\boldsymbol{A}}$ in given in (2.10). This velocity $\boldsymbol{w}$ mimics the dominant behavior of the velocity obtained in the long time scale case: as shown in the proof in Equations (A.29)-(A.30), it is actually the average $\tilde{\boldsymbol{w}} := \int_{h_{\text{bot}}}^{h_{\text{soil}}} \boldsymbol{w}\, dz$ which contributes to the effective flow in the long time scale case. By definition of $\tilde{\boldsymbol{A}}$, it holds

$$\tilde{\boldsymbol{w}} = -\Big(\int_{h_{\text{bot}}}^{h_{\text{soil}}} k_r(Q)\, dz\Big)\,\tilde{\boldsymbol{A}}\nabla\tilde{H} \simeq -\tilde{\boldsymbol{K}}(\tilde{H})\nabla_x\tilde{H}, \tag{4.4}$$

where the approximation holds because $\overline{P}_0 = \overline{Q}_0 = \rho g(\overline{H}_0 - \overline{z})$ in the long time scale case (see (3.23) and (A.38)). This later equation corresponds exactly to the 2d-horizontal Darcy law obtained in the effective problem (3.26) in the long time scale case. In particular, the vertically averaged conductivity tensor $\tilde{\boldsymbol{K}}$, defined in (2.9), corresponds to effective tensor $\overline{\boldsymbol{K}}$ in Equation (3.2).

On the other hand, as only the average $\tilde{\boldsymbol{w}}$ contributes to the effective flow in the long time scale case, numerous choices for $\boldsymbol{w}$ are possible. The only constraint being that $\tilde{\boldsymbol{w}}$ satisfies (4.4). For example it is possible to choose (instead of (2.16))

$$\boldsymbol{w} = -\frac{1}{h_{\text{soil}} - h_{\text{bot}}} \tilde{\boldsymbol{K}}(\tilde{H}) \nabla_x \tilde{H} \qquad \text{or} \qquad \boldsymbol{w} = -k_r(Q)\, \boldsymbol{M} \nabla_x \tilde{H}, \tag{4.5}$$

with $Q = \rho g(\tilde{H} - z)$ and $\boldsymbol{M}$ defined in (2.8). These choices fit well with the expected behavior in the long time scale case, and do not contribute at all in the short time scale case. Nevertheless, we want the *Fast-Slow* model to be a simple and a good approximation of the 3d-Richards model also in the *physical case*[*]: when the ratio ε of the characteristic depth to the length of the shallow aquifer remains fixed and positive. These considerations lead to discarding the choices (4.5) in favour of (2.16), indeed:

- The first choice of (4.5) is easy because $\boldsymbol{w}$ is then constant with respect to z. However this constant nature is not expected if, for example, some vertical flow holds. More precisely, in the experiment of Section 5 we have a horizontal flow in the bottom of the aquifer (because the slope of the water table), and a vertical flow holds in the upper part of the aquifer. In this case the first choice of (4.5) would lead to an unexpected horizontal flow also in the upper part.

- The second choice of (4.5) is not very simple because it leaves a dependence with respect to z through the terms Q and $\boldsymbol{M}$. This choice is better because it localizes $\boldsymbol{w}$ in the bottom part of the aquifer: where z is such that $k_r(Q) = 1$. This avoids the unexpected behavior described above. However, this choice is a bit too general in practice, the problem being that $\boldsymbol{w}$ remains non-constant with respect to z even where $k_r(Q) = 1$. This is due to $\boldsymbol{M}$ which generally depends on z. This is a drawback for implementing an efficient numerical scheme (see Remark 4.3).

- Finally, we chose $\boldsymbol{w}$ to satisfy (2.16), which describes an intermediate situation. The presence of the function $k_r(Q)$ with Q satisfying (2.13) continuously localizes $\boldsymbol{w}$ in the lower part of the aquifer. In particular, $k_r(Q)$, and hence $\boldsymbol{w}$, is small in the upper part of the domain and the corresponding velocity $\boldsymbol{v}$ is vertical. In addition $\boldsymbol{w}$ is constant with respect to z in $\{z < l\}$.

The "fast" component $\boldsymbol{u}$. The component $\boldsymbol{u}$ describes the fast component of the flow. As noted above, it coincides with the vertical component $\hat{\boldsymbol{u}}$ defined in (4.3). This definition allows a good description of the vertical transfer of water from the surface to the water table. This type of 1d-vertical flow is often used in conjonction with a 2d horizontal Dupuit-type

[*]which is not effective

flow to describe this recharge; see for example [23, 22, 20, 19]. It is important to note that here a vertical flow is allowed even in the saturated part at the bottom of the aquifer. More precisely, the first equation in (2.11) yields

$$\phi \frac{\partial s(P)}{\partial t} + \frac{\partial \boldsymbol{u} \cdot \boldsymbol{e}_3}{\partial z} = f - \mathrm{div}_x(\boldsymbol{w}), \qquad \text{in } [0,T] \times \Omega.$$

In particular in the region $\{z < l\}$, it holds $P > P_{\mathrm{sat}}$ and then $s(P) = k_r(Q) = 1$. This leads to

$$\frac{\partial \boldsymbol{u} \cdot \boldsymbol{e}_3}{\partial z} = f - \mathrm{div}(\boldsymbol{w}), \qquad \text{in } [0,T] \times \{z < l(t,\boldsymbol{x})\}, \tag{4.6}$$

where the term $\mathrm{div}(\boldsymbol{w})$ is independent of z. For example, in a situation with no source ($f = 0$), $\boldsymbol{u} \cdot \boldsymbol{e}_3$ is affine with respect to z. As we will see with the numerical experiments in Section 5, this behavior is expected in practice. This will help the *Fast-Slow* model to better approximate the 3d-Richards model. The formulation (4.6) will also aid in the numerical study of the *Fast-Slow* model.

The averaged hydraulic head $\tilde{H}$. The horizontal velocity $\boldsymbol{w}$ is characterized by the Darcy law (2.16), that is $\boldsymbol{w} = -k_r(Q)\,\tilde{\boldsymbol{A}}(\tilde{H})\nabla_x \tilde{H}$. This one is not associated with the real hydraulic head $H = P/(\rho g) + z$ but to the averaged one given in (2.14):

$$\tilde{H}(t,\boldsymbol{x}) = \fint_{h_{\mathrm{bot}}}^{l} \left(\frac{P(t,\boldsymbol{x},z)}{\rho g} + z \right) dz \qquad \text{for } (t,\boldsymbol{x}) \in [0,T[\times \Omega_{2d}.$$

The choice of a hydraulic head that is constant on z has been made to simplify the model. This particular choice is done for two reasons:

- this choice is compatible with the effective problem obtained in the long time scale case (3.23), (3.24) (3.26). Indeed, the effective pressure $\overline{P}_0$ has an affine profile on z in this effective problem. In particular the function $\overline{G}_0 : \overline{z} \mapsto \overline{P}_0/(\rho g) + \overline{z}$ is constant and coincides with the effective hydraulic head $\overline{H}_0$ from the definition (2.14) (see the proof near Equation (A.37) for more details). Note that the choice of l does not affect this compatibility with effective problems. It will, however, greatly influence the behavior of the flow in the physical geometry* Ω.
- Given the definition of l in (2.12), $\tilde{H}$ is the z-average of the hydraulic head $P/(\rho g) + z$ over the saturated part at the bottom of the aquifer. As seen before, it is this function $\tilde{H}$ which is involved in the Darcy law (2.16) which characterizes the horizontal component of flow $\boldsymbol{w}$. Since we have chosen this flow to be localized in the bottom part of the aquifer, it is natural to chose also $\tilde{H}$ to average the hydraulic head over the same part of the domain.

*for which the ratio ε of the characteristic depth to the length of the shallow aquifer remains positive

Equivalent formulation of the averaged hydraulic head. Even if the definition of $\tilde{H}$ given in (2.14) is convenient from a modeling point of view, e.g. to understand $\tilde{H}$ as an averaged hydraulic head, this formulation will be difficult to handle with in practice (especially due to the definition of l in (2.12)).

We propose an equivalent definition of $\tilde{H}$ in the following Proposition. For given functions $f :]0,T[\times\Omega \mapsto \mathbb{R}$ and $l :]0,T[\times\Omega_{2d} \mapsto \mathbb{R}$ with a graph contained in $]0,T[\times\overline{\Omega}$, we first introduce the functions $b(l,f) = b(l,f)(t,\boldsymbol{x},z)$ and $c(l) = c(l)(t,\boldsymbol{x},z)$ from $]0,T[\times\Omega$ to $\mathbb{R}$ characterized by

$$\begin{cases} -\dfrac{\partial}{\partial z}\Big(K_{zz}\dfrac{\partial}{\partial z}b(l,f)\Big) = f, & \text{in }]0,T[\times\Omega, \\ \dfrac{\partial}{\partial z}b(l,f) = 0, & \text{on }]0,T[\times\Gamma_{\text{bot}}, \\ b(l,f)(t,\boldsymbol{x},l(t,\boldsymbol{x})) = 0, & \text{on }]0,T[\times\Omega_{2d}, \end{cases} \qquad \begin{cases} \dfrac{\partial}{\partial z}\Big(K_{zz}\dfrac{\partial c(l)}{\partial z}\Big) = 0, & \text{on }]0,T[\times\Omega, \\ K_{zz}\dfrac{\partial c(l)}{\partial z} = 1, & \text{on }]0,T[\times\Gamma_{\text{bot}}, \\ c(l)(t,\boldsymbol{x},l(t,\boldsymbol{x})) = 0, & \text{on }]0,T[\times\Omega_{2d}. \end{cases} \tag{4.7}$$

We also introduce $\tilde{b}(l,f)$ and $\tilde{c}(l)$ the functions of $(t,\boldsymbol{x}) \in]0,T[\times\Omega_{2d}$ given by

$$\tilde{b}(l,f)(t,\boldsymbol{x}) = \fint_{h_{\text{bot}}(\boldsymbol{x})}^{l(t,\boldsymbol{x})} b(l,f)(t,\boldsymbol{x},z)\,dz, \quad \tilde{c}(l)(t,\boldsymbol{x}) = \fint_{h_{\text{bot}}(\boldsymbol{x})}^{l(t,\boldsymbol{x})} c(l)(t,\boldsymbol{x},z)\,dz. \tag{4.8}$$

Proposition 4.2. *Let $\tilde{H}$ be a function defined on $]0,T[\times\Omega_{2d}$ (assumed enough regular) such that*

$$\tilde{\boldsymbol{A}}(\tilde{H})\nabla_x\tilde{H}\cdot\boldsymbol{n} = 0 \quad \text{on }]0,T[\times\partial\Omega_{2d}. \tag{4.9}$$

We assume that there exists $(P,l,Q,\boldsymbol{u},\boldsymbol{v})$ satisfying (2.11)-(2.13),(2.15) and (2.16). Let $t \in]0,T[$. Then the following statements are equivalent

1. *$\tilde{H}(t,\cdot)$ satisfies (2.14) in Ω_{2d}.*
2. *$\tilde{H}(t,\cdot)$ is the unique solution of the 2d-horizontal elliptic problem on Ω_{2d}*

$$\begin{aligned} -\tilde{b}(l,1)\,\text{div}_x\big(\tilde{\boldsymbol{A}}(\tilde{H})\nabla_x\tilde{H}\big) - \tilde{c}(l)\tilde{\boldsymbol{A}}(\tilde{H})\nabla_x\tilde{H}\cdot\nabla h_{\text{bot}} + \tilde{H} \\ = \frac{P(t,\cdot,l)}{\rho g} + l + \tilde{b}(l,f) + \tilde{c}(l)f^{\text{bot}}\|\nabla_x h_{\text{bot}} - \boldsymbol{e}_3\| \quad \text{in } \Omega_{2d}. \end{aligned} \tag{4.10}$$

Proof. Let $\tilde{H}$ be a function as proposed and $(P,l,Q,\boldsymbol{u},\boldsymbol{v})$ be the associated solution of (2.11)-(2.13),(2.15) and (2.16).

Let Λ be the subset of $]0,T[\times\Omega_{2d}$ given by $\Lambda = \big\{(t,\boldsymbol{x}) \in]0,T[\times\Omega_{2d},\ l(t,\boldsymbol{x}) > h_{\text{bot}}(\boldsymbol{x})\big\}$. First, note that for $(t,\boldsymbol{x}) \in \Lambda^c$, the claimed equivalence is directly obtained. Indeed, it holds that $l = h_{\text{bot}}$, so Equation (2.14) reduces to $\tilde{H}(t,\boldsymbol{x}) = P_{h_{\text{bot}}}(t,\boldsymbol{x})/(\rho g) + h_{\text{bot}}(\boldsymbol{x})$. Moreover, we have $b(h_{\text{bot}},f) = c(h_{\text{bot}}) = 0$ on Γ_{bot} and then $\tilde{b}(h_{\text{bot}},f) = \tilde{c}(h_{\text{bot}}) = 0$, so Equation (4.10) gives exactly the same definition of $\tilde{H}$.

On the other hand let $\Omega_l^- := \big\{(t,\boldsymbol{x},z),\ z \in]h_{\text{bot}}(\boldsymbol{x}),l(t,\boldsymbol{x})[\big\} \subset \Omega$. Thanks to (2.12), we have

$$s(P) = k_r(P) = k_r(Q) = 1 \quad \text{in } \Omega_l^-. \tag{4.11}$$

Let H be the hydraulic head associated with P, we have $H(t,\boldsymbol{x},z) := P(t,\boldsymbol{x},z)/(\rho g) + z$ and, thanks to the first equation in (2.11),

$$-\frac{\partial}{\partial z}\left(K_{zz}\frac{\partial H}{\partial z}\right) = f - \mathrm{div}_x(\boldsymbol{w}) = f + \mathrm{div}_x\left(\tilde{\boldsymbol{A}}(\tilde{H})\,\nabla_x\tilde{H}\right) \quad \text{in } \Omega_l^-. \tag{4.12}$$

Moreover the third equation in (2.11) leads to $(\boldsymbol{u}+\boldsymbol{w})\cdot\boldsymbol{n} = f^{\mathrm{bot}}$. As $\boldsymbol{n} = (\nabla_x h_{\mathrm{bot}} - \boldsymbol{e}_3)/\|\nabla_x h_{\mathrm{bot}} - \boldsymbol{e}_3\|$ we get

$$\left(K_{zz}\frac{\partial H}{\partial z}\right)\Big|_{z=h_{\mathrm{bot}}} = \tilde{\boldsymbol{A}}(\tilde{H})\,\nabla_x\tilde{H}\cdot\nabla_x h_{\mathrm{bot}} + f^{\mathrm{bot}}\,\|\nabla_x h_{\mathrm{bot}} - \boldsymbol{e}_3\| \quad \text{on } \Lambda. \tag{4.13}$$

Then, for each $(t,\boldsymbol{x}) \in \Lambda$, the function $H = H(t,\boldsymbol{x},\cdot)$ is characterized on $[h_{\mathrm{bot}}(\boldsymbol{x}), l(t,\boldsymbol{x})]$ as the unique solution of the 1d-vertical linear elliptic problem (4.12) associated with the Neumann condition (4.13) on Γ_{bot} and with the Dirichlet condition on $\{z = l(t,\boldsymbol{x})\}$ given by

$$H\big(t,\boldsymbol{x},l(t,\boldsymbol{x})\big) = \frac{P_l(t,\boldsymbol{x})}{\rho g} + l(t,\boldsymbol{x}), \tag{4.14}$$

where P_l is introduced in (2.13). Then, for all $(t,\boldsymbol{x}) \in \Lambda$, we write H on $[h_{\mathrm{bot}}(\boldsymbol{x}), l(t,\boldsymbol{x})]$ as the following linear combination of the elementary functions b and c defined in (4.8)

$$H = \frac{P_l}{\rho g} + l + b(l,1)\,\mathrm{div}_x\left(\tilde{\boldsymbol{A}}(\tilde{H})\nabla_x\tilde{H}\right) + b(l,f) + c(l)\big(\tilde{\boldsymbol{A}}(\tilde{H})\nabla\tilde{H}\cdot\nabla_x h_{\mathrm{bot}} + f^{\mathrm{bot}}\|\nabla_x h_{\mathrm{bot}} - \boldsymbol{e}_3\|\big). \tag{4.15}$$

By averaging vertically Equation (4.15) over $[h_{\mathrm{bot}}, l]$, we get

$$\begin{aligned} -\tilde{b}(l,1)\,\mathrm{div}_x\left(\tilde{\boldsymbol{A}}(\tilde{H})\nabla_x\tilde{H}\right) - \tilde{c}(l)\tilde{\boldsymbol{A}}(\tilde{H})\nabla_x\tilde{H}\cdot\nabla h_{\mathrm{bot}} + \fint_{h_{\mathrm{bot}}}^{l} H(\cdot,\cdot,z)\,dz \\ = \frac{P_l}{\rho g} + l + \tilde{b}(l,f) + \tilde{c}(l)\,f^{\mathrm{bot}}\|\nabla_x h_{\mathrm{bot}} - \boldsymbol{e}_3\| \quad \text{in } \Lambda. \end{aligned} \tag{4.16}$$

It follows the equivalence claimed in Proposition 4.2.

□

Remark 4.3. *The characterization of H in* (4.15) *is possible since $k_r(Q)$ is constant with respect to z in $]h_{\mathrm{bot}}, l[$. This is due to the proposed choice of $\boldsymbol{w}$ satisfying* (2.16)*, combined with the auxiliary pressure Q given in* (2.13).

We deduce from Proposition 4.2 that the *Fast-Slow* model (2.11)–(2.16) is equivalent to that in which Equation (2.14) is replaced by Equation (4.10). The regularity of $\tilde{H}$, ensured by the ellipticity of Equation (4.10), makes this system a numerically efficient alternative to (2.14).

4.4. The *Fast-Slow* model as a 1d-2d coupling model

As mentioned before, the *Fast-Slow* model (2.11)–(2.16) serves the three purposes given in Property 2.1. In this part, we propose a new formulation that will help the numerical implementation. It is a necessary step to satisfy the third point of Property 2.1.

The system (2.11)–(2.16) implies that (P, u_3) satisfies

$$\begin{cases} \phi \dfrac{\partial s(P)}{\partial t} + \dfrac{\partial u_3}{\partial z} = f - \mathrm{div}_x(\boldsymbol{w}) & \text{in }]0,T[\times\Omega \\ u_3 = -k_r(P)\, K_{zz}\Big(\dfrac{1}{\rho g}\dfrac{\partial P}{\partial z} + 1\Big) & \text{in }]0,T[\times\Omega \\ \alpha\, P + \beta\, u_3\, \boldsymbol{e}_3 \cdot \boldsymbol{n} = f_{\mathrm{soil}} - \beta\, \boldsymbol{w}\cdot\boldsymbol{n} & \text{in }]0,T[\times\Gamma_{\mathrm{soil}} \\ u_3\, \boldsymbol{e}_3 \cdot \boldsymbol{n} = f_{\mathrm{bot}} - \boldsymbol{w}\cdot\boldsymbol{n} & \text{in }]0,T[\times\Gamma_{\mathrm{bot}} \\ \boldsymbol{v}\cdot\boldsymbol{n} = 0 & \text{on }]0,T[\times\Gamma_{\mathrm{ver}} \\ P(0,\boldsymbol{x},z) = P_{\mathrm{init}}(\boldsymbol{x},z) & \text{for } (\boldsymbol{x},z)\in\Omega. \end{cases} \tag{4.17}$$

This problem can be viewed as a collection of 1d-vertical Richards problems describing the flow in each water column, parameterized by the horizontal position $\boldsymbol{x} \in \Omega_{2d}$. The term $\mathrm{div}_x(\boldsymbol{w})$ in the first equation plays the role of a source term, quantifying the amount of water entering or leaving the column (at each height) due to horizontal flow. The system (4.17) is coupled to the other equations of (2.11)–(2.16), which characterize in particular $\tilde{H}$ and $\boldsymbol{w}$ in terms of P. In practice, the characterization of $\tilde{H}$ given in (4.10) will be used.

In summary, the *Fast-Slow* model is seen as the coupling of independent 1d-Richards problems in the entire domain Ω with a 2d-horizontal elliptic problem characterizing the horizontal flow. The scheme will alternate the resolution of these two problems and a significant reduction in computational time is expected and observed compared to the resolution of the full 3d-Richards problem (see Section 6 for more details on the scheme).

4.5. Possible variants of the *Fast-Slow* model

In this section, we propose possible variants of the *Fast-Slow* model. All of these variants are designed to satisfy the three criteria given in Property 2.1 (as the *Fast-Slow* model).

Another definition of $\boldsymbol{w}$. In the first variant, we replace the definition of the auxiliary pressure Q in (2.13) with the following:

$$Q(t,\boldsymbol{x},z) = \rho g\big(\tilde{H}(t,\boldsymbol{x}) - z\big). \tag{4.18}$$

It is easy to adapt the proof of Theorem 3.1 to this new definition. Indeed, in this case, equation (4.4) becomes (thanks to (2.10))

$$\tilde{\boldsymbol{w}} = -\Big(\int_{h_{\mathrm{bot}}}^{h_{\mathrm{soil}}} k_r(Q)\, dz\Big)\, \tilde{\boldsymbol{A}}\nabla\tilde{H} = -\tilde{\boldsymbol{K}}(\tilde{H})\nabla_x\tilde{H},$$

where the last relation is now a perfect equality. It follows that this variant is also a good approximation of the 3d-Richards model in shallow aquifers.

On the other hand, as $k_r(Q)$ is still constant with respect to z in the lower part of the aquifer, the strategy described in Subsection 4.4 could be adapted to this case. Point (iii) follows.

However, this choice implies that the horizontal flow is localized in the domain $z < \tilde{H} - P_{\text{sat}}/(\rho g)$ (where $k_r(Q) \sim 1$) instead of the domain $z < l$. This is a major drawback for the model to satisfy the point (ii) above. This justifies our preference for the choice (2.13) to define the auxiliary pressure Q.

Another choice of level l. In Equation (2.12), we choose the level l to be the lowest level such that $P = P_{\text{sat}}$. The domain $\{z < l\}$ then represents the water table at the bottom of the aquifer.

In fact, as already noted, this choice has no effect on the effective problems (3.22)–(3.26) (l does not appear in them). In particular the results of Theorem 3.1 are still true if a different choice of level $l \in [h_{\text{soil}}, h_{\text{bot}}]$ is made.

The main disadvantage of any other choice for l is that the soil may be unsaturated in the lower part of the aquifer $\{z < l\}$. In this case the property (4.11) is false and the characterization of $\tilde{H}$ as a solution to an elliptic problem may fail. We will discuss this point in the next paragraph.

On the other hand, a different choice of l may help the numerical resolution of the problem. The original definition of l in (2.12) is indeed highly dependent on P and can lead to instabilities and oscillations during the numerical treatment.

The averaged hydraulic head $\tilde{H}$ as a solution to an elliptic problem. As shown in Subsection 4.4, $\tilde{H}$ is defined in (2.14) and is equivalently characterized as the unique solution of the elliptic problem (4.10). The equivalence is true because the definition (2.12) of l holds. It is then possible to replace Equation (2.14) by (4.10) in the definition of the coupled problem. The idea is to keep this characterization of $\tilde{H}$ even if a different definition of level l is chosen, as proposed in the previous variant. A good compromise is to relax the definition of l with

$$l(t, \boldsymbol{x}) \simeq \inf\Big\{ z \in [h_{\text{bot}}(\boldsymbol{x}), h_{\text{soil}}(\boldsymbol{x})],\ P(t, \boldsymbol{x}, z) \leq P_{\text{sat}} \Big\}. \tag{4.19}$$

Finally any variant of the *Fast-Slow* model consisting of the equations (2.11), (2.13), (2.15), (2.16), (4.10) and associated with a level l satisfying (4.19) will be such that:

- it admits the effective problems (3.22)–(3.26). In particular, Theorem (3.1) also holds for this variant. In this sense, a solution of such a variant approximates the solution of the original 3d-Richards problem in shallow aquifers.
- it is still mass-conservative in the sense of Proposition 4.1.
- since (4.19) holds, the lower part of the aquifer $\{z < l\}$ represents approximately the saturated part at the bottom of the aquifer. It follows that the physical interpretations given in Subsections 4.2 and 4.3 are globally unchanged.
- a good choice of relaxation in the definition of l may allow to avoid critical oscillations in the numerical treatment of the problem. This significantly improves the convergence of the Picard fixed-point algorithm described below (Subsection 6.2).
- we keep the structure of coupling 1d-verticals problems with a 2d-horizontal one. This variant is still efficient to save time during the numerical resolution.

It is this type of variant that will be used for the numerical simulations in the next part (see Section 5 and Section 6).

5. NUMERICAL SIMULATIONS

In this section we aim to quantify the differences between the flows described by the original 3d-Richards model and the new *Fast-Slow* model respectively. Special attention is paid to the case of a geometry that is not particularly shallow combined with a non-constant bedrock level h_{bot}. Indeed, for shallow aquifers, similar behaviors are expected : consequence of Theorem 3.1.

5.1. Description of the experiment

Geometry and time interval. We consider a cylindrical geometry as described in Subsection 2.1. To improve the vizualisation of the results, we consider a 2d-domain in which the horizontal part Ω_{2d} is the interval $]0, L[$ with $L > 0$. On the other hand, in this article we focus on the modeling of the flow in the subsurface. We will simplify the geometry by considering the constant soil level $h_{\text{soil}} = 0$. Conversely, the level $h_{\text{bot}} < 0$, which represents the level of the bedrock at the bottom of the aquifer, is chosen to be non-constant (to show the influence of these variations on the flow). The 3d-domain reads as

$$\Omega = \big\{(x,z) \in]0,L[\times\mathbb{R}, \quad z \in \big]h_{\text{bot}}(\boldsymbol{x}), 0\big[\big\}.$$

We choose $L = 30$m and the total experiment time $T = 14$h. The exact definition of h_{bot} is given in the Appendix, Subsection A.1.

Physical parameters. The numerical experiment uses the following set of physical data. In particular, the soil is assumed to be homogeneous and isotropic. Let $\boldsymbol{I}_3$ the 3×3 identity matrix. We set

$$s(P) = (P_{\text{sat}}/P)^{\lambda}, \quad k_r(P) = (P_{\text{sat}}/P)^{2+3\lambda}, \quad P_{\text{sat}} = -2000 \text{ Pa}, \quad \lambda = 3,$$
$$\rho = 10^3 \text{ kg}\cdot\text{m}^{-3}, \quad \phi = 0.3, \quad \boldsymbol{K}_0 = k_0 \boldsymbol{I}_3, \quad k_0 = 3.10^{-5} \text{ m}\cdot\text{s}^{-1}.$$

In particular, these choices for the water content function $s(P)$ and the soil conductivity $k_r(P)$ correspond to the classical Brooks and Corey model [1].

Sources and boundary conditions. The source term f in (2.6) and (2.11) collects the contributions of water injection at three locations of the domain and water pumping at another one, see Figure 1. We also choose a non-vanishing term f^{bot} in (2.7) and (2.11). This corresponds to a bedrock at the bottom of the aquifer that is not perfectly impermeable. Finally, we consider an aquifer without interaction with overlying water. For this purpose, we choose a homogeneous Neumann condition on Γ_{soil}, which is then associated with $\alpha = 0$, $\beta = 1$ and $f^{\text{soil}} = 0$ in (2.7) and (2.11). A homogeneous Neumann condition is also chosen on Γ_{ver}. The exact definition of f and f^{bot} is given in the Appendix (see A.1).

Initial data. The initial pressure is characterized for all $(x,z) \in \Omega$ by

$$P(0,\boldsymbol{x},z) = \max\{\rho g(h(\boldsymbol{x})-z) + P_{\text{sat}}, P_{\min}\}, \qquad P_{\min} = -10000 \text{ Pa}. \tag{5.1}$$

The level $z = h$ represents the saturated/unsaturated interface where $h > h_{\text{bot}}$. In this particular situation, the right part of the domain is completely unsaturated, with a corresponding $h < h_{\text{bot}}$. We show the initial saturation in the first image of Figure 1. The exact definition of h is given in the appendix (see A.1).

5.2. Reference flow characterized by 3d-Richards model

The purpose of this Subsection is to comment on the reference flow obtained by the full 3d-Richards model* associated with the physical data and the initial situation given above.

In Figure 1 we show the soil saturation $s(P)$ and the velocity field $\boldsymbol{v}$. More precisely there are four images in Figure 1 corresponding to times (in hours): $t = 0$, $t \simeq 4.5$, $t = 10.5$ and $t = 14$ respectively. In each of them, we use two grayscales to represent the soil saturation and the lower boundary condition :

- in the upper part $z > h_{\text{bot}}$ (that is in Ω), the gray scale represents the saturation of the porous media; the white is for dry regions of the soil and the dark gray for saturated ones,
- in the lower part $z < h_{\text{bot}}$ (below the domain), the gray scale represents the source term $f^{\text{bot}} = f^{\text{bot}}(\boldsymbol{x})$; the dark gray corresponds to $f^{\text{bot}} = 0$ (impermeable bedrock) and the light gray corresponds to a negative value of f^{bot} (inhomogeneous Neumann condition). In this case the water flow is outgoing.

In each image of Figure 1, the black arrows represent the velocity field $\boldsymbol{v}$. In addition, we represent the location of the injection zones by dashed lines and the location of the pumping zone by a solid line. Let us give some comments on each image.

The initial situation $t = 0$. It is shown in the upper left image of Figure 1.

The upper level of the water table (interface saturated/unsaturated) has a roughly gaussian shape with a maximum near $x = 10$. This non-constant level of the water table causes a flow of water that tends to level it.

Two injection zones are located in the upper part of the domain, well over the water table. No water has been injected in this initial situation. There is also an injection zone on the top left of the water table. This presence accounts for the long arrow.

There is also a pumping zone in the right part of the aquifer, near the bedrock. This pump causes a water flow in the column above the pump. At this stage of the experiment, the water velocity is still almost vertical.

The bedrock is mostly impermeable ($f^{\text{bot}} = 0$) except near $x = 12$ where a non-vanishing outflow is imposed. The corresponding water leakage is well visible in this region at the bottom of the aquifer. Moreover, the fact that the bedrock in the left part of the aquifer is impermeable is also consistent with the water flux $\boldsymbol{v}$ that is parallel to h_{bot}.

*In fact, it is a simplified 2d situation

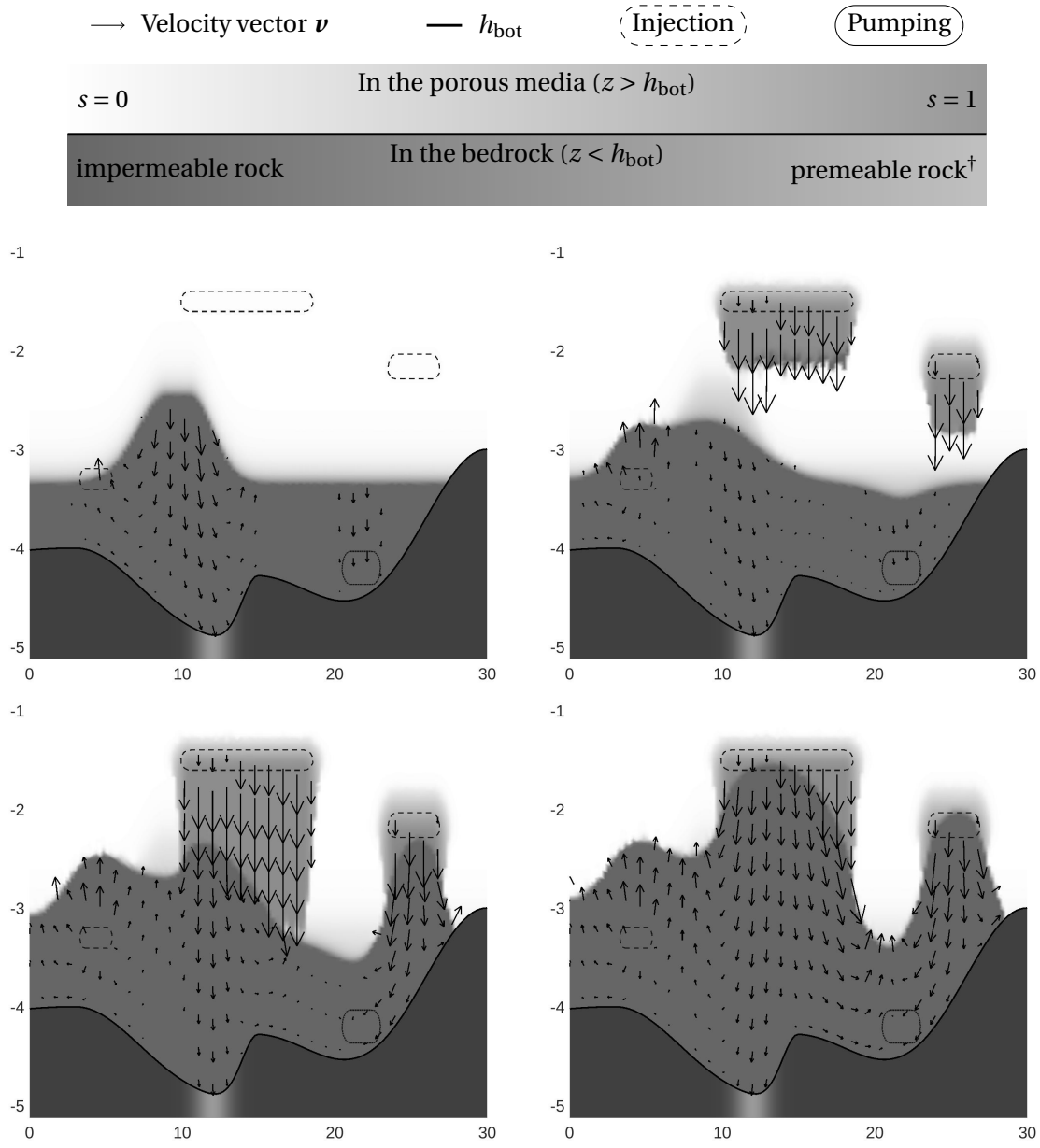

Figure 1: Numerical solutions of the 3d-Richards equations in the situation described in Subsection 5.1 for $t \simeq$ 0h, $t \simeq$ 4h30, $t \simeq$ 10h30 and $t \simeq$ 14h.

[2] corresponds to non-vanishing flux condition on h_{bot}

The second time $t = 4h30$. The corresponding solution is shown in the upper right image of figure 1.

The upper level of the water table near $x = 10$ is much lower. This is due to the natural flattening of the water table as well as the leakage where $f^{\text{bot}} \neq 0$.

On the other hand, the water injection in the left part has filled the water table which sees its level rise significantly.

Near the two highest injection zones, the ground is wet enough to allow water to flow down by gravity. The flow here is nearly vertical.

Pumping in the right part has caused the water table to drop down. The flow here is no longer vertical, but has a small horizontal component.

Times $t = 10h30$ and $t = 14h$. We show the corresponding solutions in the lower left and right images of Figure 1.

Water flowing down from the two highest injection zones has reached the table. It follows the rise of the water table, especially in the right part of the domain, where the water table was initially empty. Moreover, the flow velocity increases in the water table while remaining parallel to the impermeable bedrock.

The same increase also appears near the injection zone in the left part of the aquifer.

Similarity with the *Fast-Slow* model. It is important to note that the behavior of the flow, characterized by the 3d-Richards model, seems to agree with the properties of the *Fast-Slow* model shown in Section 4, regardless of the sources in this particular experiment. More precisely we have, at least qualitatively:

- in the upper part of the domain, above the water table, the water flow is almost vertical.
- in the water table, the velocity exhibits a non-vanishing vertical component that depends on the depth. We can also see that this vertical component is nearly affine with respect to z. This is the behavior imposed by the construction of $\boldsymbol{u}$ in the *Fast-Slow* model. Moreover, for any $x \in \Omega_{2d}$, the horizontal component of the velocity seems to be constant with respect to z; as $\boldsymbol{w}$ in the *Fast-Slow* model.

5.3. Velocities and water table comparison

In this Subsection, we compare the 3d-Richards and *Fast-Slow* models by computing their respective solution in the particular situation described and commented on in the last two Subsections. The results are shown in Figure 2 and correspond to the same times as in Figure 1. More precisely, on each frame of Figure 2:

- the domain Ω is not shown completely, we focus on the lower part of the aquifer to improve the visualisation.
- the grayscale represents the saturation $s(P)$ associated with the solution of the *Fast-Slow* model. As in Figure 1, the dark gray represents the saturated soil and the white represents the dry soil. In particular, we do not overlay the saturation associated with the 3d-Richards model.

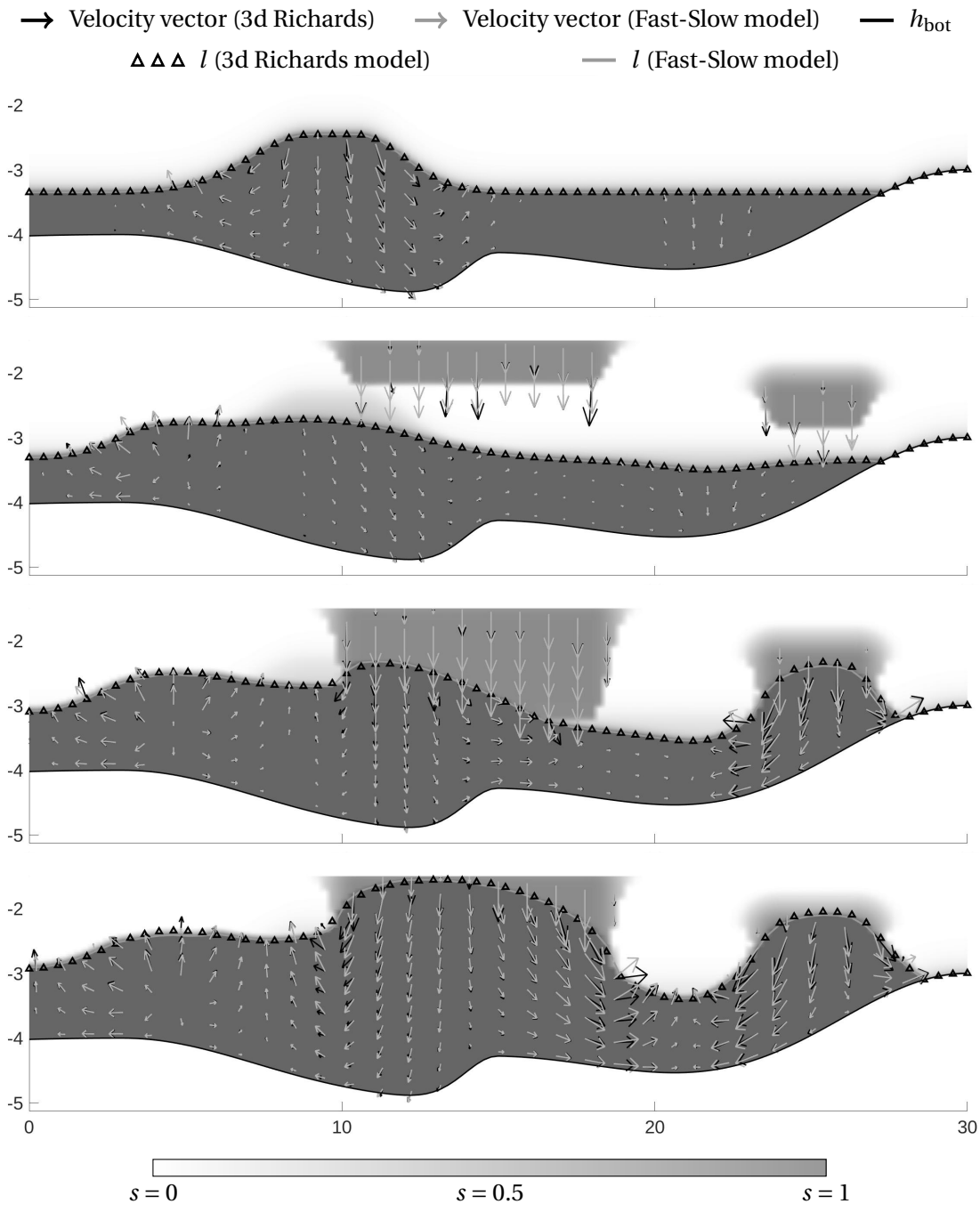

Figure 2: Comparison of the 3d-Richards model and of the *Fast-Slow* model for $t \simeq$ 0h, $t \simeq$ 4h30, $t \simeq$ 10h30 and $t \simeq$ 14h.

- we do not show the pumping and injection zones to clarify the drawings.
- we show the upper level of the water table associated with each model. We use black triangles for the 3d-Richards model and a gray solid line for the new model.
- we use black and gray arrows to represent the velocity field of the fluid. They are associated with the solution of the 3d-Richards* and of the *Fast-Slow* model respectively.

Above the water table. In this example, it should be noted that the dominant component of the flow in the upper part of the aquifer is vertical. It follows that the *Fast-Slow* model is efficient in this situation. Indeed, it is tuned to neglect the horizontal component and to capture well the vertical component in this part of the domain. More precisely the horizontal component of the velocity field is $\boldsymbol{w}$, defined in (2.16), and is small in the upper part of the aquifer (see comments of Subsection 4.3). At the same time the vertical component is $\boldsymbol{u}$ and roughly satisfies a 1d-Richards problem (vertical) wherever $\boldsymbol{w}$ is small (see equations (2.11) and (2.16)).

The two models then produce very similar velocity fields in the upper part of the domain as it can be seen in the last three frames of Figure 2.

Inside the water table. As expected and commented on in Subsection 4.3, the flow characterized by the *Fast-Slow* model in the water table (for $z \leq l(t,\boldsymbol{x})$) is such that:

- the horizontal component of the velocity $\boldsymbol{w} = \tilde{A}(\tilde{H})\nabla_x \tilde{H}$ is constant with respect to z (see equations (2.13) and (2.16)),
- the vertical component $\boldsymbol{u} = u_3\,\boldsymbol{e}_3$ satisfies the 1d-Richards problem (4.17). In particular, it exhibits an affine profile with respect to z far from the sources (where $f \simeq 0$).

As we can see in Figure 1, the 3d-Richards flow has mostly the same velocity profile. In particular the *Fast-Slow* model takes well into account the effects of injection, pumping and of the Neumann condition on h_{bot} (homogeneous or not). Since the velocity field is well described, this is also the case for the water table level l.

Of course there are still some differences between the models. They are localized in the water columns close to where the water table has a steep slope. In these regions one can observe that the 3d-Richards velocity exhibits a horizontal component that depends on z; with larger values at the top of the water table. By construction, the *Fast-Slow* model is unable to fit this behavior. In fact, these differences are not surprising in this particular example. Indeed, the *Fast-Slow* model is tuned to be a good approximation when the aquifer is shallow (as shown in Theorem 3.1). In this example, the aquifer has a ratio of $\varepsilon = 1/6$ which is far from being small. The experiment shown in Figure 2 shows that the *Fast-Slow* model can still be a good approximation for such aquifers.

Remark 5.1. *As briefly explained in the introduction, the coupled model proposed in [23] is also made to approximate the flow in shallow aquifers. In fact, it also presents the effective*

*in particular, the black arrows in Figure 2 are exactly the same as those of Figure 1

problems (3.22)–(3.26) *when the ratio of the horizontal length to the depth of the aquifer tends to zero. This model has the behavior described in Property 1.1 and it could be used to describe the flow in the situation presented in Subsection 5.1. In this case the flow in the upper part of the aquifer, assumed to be purely vertical where $z > l$, would be very close to that obtained with the Fast-Slow model. The main difference would be in the lower part of the aquifer where the model of [23] is assumed to be purely horizontal.*

6. NUMERICAL SCHEME

6.1. Fully implicit time scheme

We perform a time discretization of the system (2.11)–(2.16). For a fixed $M \in \mathbb{N}^*$, we introduce the discrete time $t^n = n\Delta_t$ with $n = \{0, ..., M\}$ and $\delta_t = T/M$. For all $n \in \{0, ..., M\}$, the discrete unknowns at time t^n are denoted by the superscript ^{n}; in particular, for all $(x, z) \in \Omega$, we have

$$P^n(x,z) \simeq P(t^n, \boldsymbol{x}, z), \quad \boldsymbol{u}^n(x,z) \simeq \boldsymbol{u}(t^n, \boldsymbol{x}, z), \quad \boldsymbol{w}^n(x,z) \simeq \boldsymbol{w}(t^n, \boldsymbol{x}, z), \quad l^n(\boldsymbol{x}) \simeq l(t^n, \boldsymbol{x}).$$

Implicit scheme. We have $P^0 = P_{\text{init}}$ in Ω. Let $n \in \{1, \dots, M\}$. We use a backward Euler method to approximate the time derivative in (2.11)–(2.16), with the variant where (2.14) is replaced by (4.10). It follows the next fully implicit time scheme which consists of finding the discrete pressure $P^n = P^n(x, z)$ such that

$$\begin{cases} \phi \dfrac{s(P^n) - s(P^{n-1})}{\delta_t} + \dfrac{\partial}{\partial z}(\boldsymbol{u}^n \cdot \boldsymbol{e}_3) + \operatorname{div}_x(\boldsymbol{w}^n) = f^n & \text{in } \Omega \\ \boldsymbol{u}^n = -k_r(P^n)\, K_{zz} \Big(\dfrac{1}{\rho g} \dfrac{\partial P^n}{\partial z} + 1 \Big) \boldsymbol{e}_3, & \text{in } \Omega \\ \alpha\, P^n + \beta\, (\boldsymbol{u}^n + \boldsymbol{w}^n) \cdot \boldsymbol{n} = f^{\text{soil},n} & \text{in } \Gamma_{\text{soil}} \\ (\boldsymbol{u}^n + \boldsymbol{w}^n) \cdot \boldsymbol{n} = f^{\text{bot},n} & \text{in } \Gamma_{\text{bot}} \\ \boldsymbol{w}^n \cdot \boldsymbol{n} = 0 & \text{in } \Gamma_{\text{ver}} \end{cases} \tag{6.1}$$

$$l^n(\boldsymbol{x}) = \inf \Big\{ z \in [h_{\text{bot}}(\boldsymbol{x}), h_{\text{soil}}(\boldsymbol{x})],\ P^n(t, \boldsymbol{x}, z') \le P_{\text{sat}} \Big\} \quad \text{in } \Omega_{2d}, \tag{6.2}$$

$$\begin{aligned} -\tilde{b}(l^n, 1)\, \operatorname{div}_x \big(\tilde{\boldsymbol{A}}(\tilde{H}^n) \nabla_x \tilde{H}^n \big) - \tilde{c}(l^n) \tilde{\boldsymbol{A}}(\tilde{H}^n) \nabla_x \tilde{H}^n \cdot \nabla h_{\text{bot}} + \tilde{H}^n \\ = H^n(\cdot, l^n) + \tilde{b}(l^n, f^n) + \tilde{c}(l^n) f^{\text{bot},n} \| \nabla_x h_{\text{bot}} - \boldsymbol{e}_3 \| \quad \text{in } \Omega_{2d}. \end{aligned} \tag{6.3}$$

$$Q^n(\boldsymbol{x}, z) = P^n(t, \boldsymbol{x}, l^n(t, \boldsymbol{x})) + \rho g (l^n - z), \quad \boldsymbol{w}^n = -k_r(Q^n)\, \tilde{\boldsymbol{A}}(\tilde{H}^n) \nabla_x \tilde{H}^n \quad \text{in } \Omega. \tag{6.4}$$

Mass conservation. By construction, we have the following mass conservation result. It is easily obtained by integrating the first equation in (6.1) over Ω, followed by an integration by parts and using of the boundary conditions.

Proposition 6.1. *Let $(P_n)_{n=0}^M$ be the discrete solution of the system* (6.1)–(6.4) *below. Then for all $n \in \{1, \dots, M\}$ it holds*

$$\int_\Omega \phi \big(s(P^n) - s(P^{n-1}) \big)\, dx\, dz = \delta_t \Big(\int_\Omega f^n\, dx\, dz - \int_{\Gamma_{\text{bot}}} f^{\text{bot},n}\, dx\, dz - \int_{\Gamma_{\text{soil}}} (\boldsymbol{u}^n + \boldsymbol{w}^n) \cdot \boldsymbol{n}\, dx\, dz \Big).$$

In addition to this mass-conservation property, the fully implicit time scheme is more stable than a naive explicit or semi-implicit scheme. This justifies its consideration. Of course this scheme is 3d and strongly nonlinear. The rest of this section is devoted to obtaining a practical implementation of the implicit time scheme (6.1)–(6.4). In particular a key goal is to obtain a procedure that avoids solving any 3d problems.

6.2. Picard fixed-point algorithm

For a given $n \in \{1,\dots,M\}$ we assume to know P^{n-1} and then $\tilde{H}^{n-1}$, l^{n-1} and

$$g^n := f^n - \frac{\phi}{\delta_t}\big(1 - s(P^{n-1})\big).$$

We construct the sequence $(P^{n_p}, \tilde{H}^{n_p}, l^{n_p})_p$ with $(P^{n_0}, \tilde{H}^{n_0}, l^{n_0}) = (P^{n-1}, \tilde{H}^{n-1}, l^{n-1})$ and such that for all $p \in \mathbb{N}^*$:

- the auxiliary pressure is: $Q^{n_{p-1}}(t,\boldsymbol{x},z) = P^{n_{p-1}}(t,\boldsymbol{x},l^{n_{p-1}}(t,\boldsymbol{x})) + \rho g(l^{n_{p-1}} - z)$, in Ω_{2d}.
- the horizontal velocity is: $\boldsymbol{w}^{n_{p-1}} = -k_r(Q^{n_{p-1}})\,\tilde{\boldsymbol{A}}(\tilde{H}^n)\,\nabla_x \tilde{H}^{n_{p-1}}$.
- the pressure P^{n_p} is the unique solution of the following 1d-Richards problems, where $x \in \Omega_{2d}$ is a parameter

$$\begin{cases} \phi\dfrac{s(P^{n_p}) - s(P^{n-1})}{\delta_t} + \dfrac{\partial}{\partial z}(\boldsymbol{u}^{n_p}\cdot\boldsymbol{e}_3) = f^n - \mathrm{div}_x(\boldsymbol{w}^{n_{p-1}}) & \text{in } \Omega \\ \boldsymbol{u}^{n_p} = -k_r(P^{n_p})\,K_{zz}\Big(\dfrac{1}{\rho g}\dfrac{\partial P^{n_p}}{\partial z} + 1\Big)\boldsymbol{e}_3, & \text{in } \Omega \\ \alpha\,P^{n_p} + \beta\,\boldsymbol{u}^{n_p}\cdot\boldsymbol{n} = f^{\mathrm{soil},n} - \beta\,\boldsymbol{w}^{n_{p-1}}\cdot\boldsymbol{n} & \text{in } \Gamma_{\mathrm{soil}} \\ \boldsymbol{u}^{n_p}\cdot\boldsymbol{n} = f^{\mathrm{bot},n} - \boldsymbol{w}^{n_{p-1}}\cdot\boldsymbol{n} & \text{in } \Gamma_{\mathrm{bot}} \end{cases} \tag{6.5}$$

- the corresponding isolevel l^{n_p} reads as

$$l^{n_p}(\boldsymbol{x}) := \inf\big\{z \in [h_{\mathrm{bot}}(\boldsymbol{x}), h_{\mathrm{soil}}(\boldsymbol{x})],\ P^{n_p}(t,\boldsymbol{x},z) < P_{\mathrm{sat}}\big\}. \tag{6.6}$$

- We compute the functions $\tilde{b}(l^{n_p},1)$, $\tilde{b}(l^{n_p},g^n)$ and $\tilde{c}(l^{n_p})$.
- the averaged hydraulic head $\tilde{H}^{n_p}$ is the unique solution of the 2d horizontal problem:

$$\begin{cases} -\tilde{b}(l^{n_p},1)\,\mathrm{div}_x\big(\tilde{\boldsymbol{A}}(\tilde{H}^{n_p})\nabla_x\tilde{H}^{n_p}\big) - \tilde{c}(l^{n_p})\tilde{\boldsymbol{A}}(\tilde{H}^{n_p})\nabla\tilde{H}^{n_p}\cdot\nabla h_{\mathrm{bot}} + \tilde{H}^{n_p} = G^{n_p}, & \text{on } \Omega_{2d} \\ \tilde{\boldsymbol{A}}(\tilde{H}^{n_p})\nabla_x\tilde{H}^{n_p}\cdot\boldsymbol{n} = 0 & \text{on } \partial\Omega_{2d}, \end{cases} \tag{6.7}$$

  where $G^{n_p} : \Omega_{2d} \mapsto \mathbb{R}$ is given by

$$G^{n_p} = \frac{1}{\rho g}P^{n_p}(t,\boldsymbol{x},l^{n_p}(t,\boldsymbol{x})) + l^{n_p} + \tilde{b}(l^{n_p},g^n) + \tilde{c}(l^{n_p})f^{\mathrm{bot},n}\|\nabla_x h_{\mathrm{bot}} - \boldsymbol{e}_3\| \qquad \text{on } \Omega_{2d}.$$

Let $n \in \{1,\dots,M\}$. By construction, if this sequence $(P^{n_p}, \tilde{H}^{n_p}, l^{n_p})$ converges, it converges to $(P^n, \tilde{H}^n, l^n)$ the solution of problem (6.1)–(6.4) associated with the fully implicit time scheme.

Remark 6.2. *We note that in the numerical simulations given in Section 5, a variant of the Fast-Slow model was used (has described in the last paragraph of Subsection 4.5). It consists in relaxing the definition of the level l^n in* (6.2) *to improve the numerical stability of the Picard fixed-point algorithm. In practice, Equation* (6.6) *is replaced by*

$$l^{n_p}(\boldsymbol{x}) := \max\{l^{n_{p-1}}, h^{n_p}\},$$

where $h^{n_p}(\boldsymbol{x}) := \inf\left\{z \in [h_{\text{bot}}(\boldsymbol{x}), h_{\text{soil}}(\boldsymbol{x})],\ P^{n_p}(\boldsymbol{x}, z) < P_{\text{sat}}\right\}$.

Computational time. The scheme presented above then alternates solving of a collection of 1d-vertical Richards problems with solving a 2d-horizontal elliptic problem. At each step, the 1d problems are independent and can be solved in parallel. The choice described in Remark 6.2 makes the Picard fixed-point fast converging. The resulting procedure leads to a very fast resolution.

For example, the 1000 time steps computed for the numerical simulation of Section 5 (using a grid made of 130 × 130 nodes to mesh Ω) are obtained in about 10 seconds. These computations are done on a personal computur using C++ code that is not yet parallelized.

ACKNOWLEDGEMENTS

Experiments presented in this paper were carried out using the computing platform CALCULCO, which is supported by SCoSI/ULCO (Service COmmun du Système d'Information de l'Université du Littoral Côte d'Opale).

APPENDIX

A.1. Precise definition of the data used in the numerical simulations

Source terms. Let us define the function g for $(y, a, b, \sigma, \xi) \in \mathbb{R}^5$ by

$$g(y,a,b,\sigma,\xi) = \begin{cases} e^{-\frac{(y-a)^2}{\sigma^2}} & \text{if } y < a \\ e^{-\frac{(y-b)^2}{\xi^2}} & \text{if } y > b \\ 1 & \text{if not} \end{cases}$$

Moreover, we introduce functions f^i for $i \in \{1,2,3,4\}$ and $(x,z) \in \mathbb{R}^2$ by

$$f^i(x,z) := \alpha^i\, g(x, a_x^i, b_x^i, \sigma_x^i, \xi_x^i)\, g(z, a_z^i, b_z^i, \sigma_z^i, \xi_z^i),$$

with

$$\alpha^1 = -10^{-5}, \quad a_x^1 = 0.7\,L, \quad b_x^1 = 0.75\,L, \quad \sigma_x^1 = \xi_x^1 = 0.02\,L, \quad a_z^1 = b_z^1 = -4.2, \quad \sigma_z^1 = \xi_z^1 = 0.2,$$
$$\alpha^2 = 3\,10^{-5}, \quad a_x^2 = 0.8\,L, \quad b_x^2 = 0.88\,L, \quad \sigma_x^2 = \xi_x^2 = 0.02\,L, \quad a_z^2 = b_z^2 = -2.2, \quad \sigma_z^2 = 0.1, \quad \xi_z^2 = 0.2,$$
$$\alpha^3 = 3\,10^{-5}, \quad a_x^3 = 0.12\,L, \quad b_x^3 = 0.17\,L, \quad \sigma_x^3 = \xi_x^3 = 0.02\,L, \quad a_z^3 = b_z^3 = -3.3, \quad \sigma_z^3 = \xi_z^3 = 0.2,$$
$$\alpha^4 = 3\,10^{-5}, \quad a_x^4 = 0.35\,L, \quad b_x^4 = 0.6\,L, \quad \sigma_x^4 = \xi_x^4 = 0.02\,L, \quad a_z^4 = b_z^4 = -1.5, \quad \sigma_z^4 = \xi_z^4 = 0.1?$$

For for all $(t,\boldsymbol{x},z) \in]0,T[\times\Omega$ we set $f(t,\boldsymbol{x},z) = \sum_{k=1}^4 f^i(x,z)$ and

$$f^{\rm bot}(t,\boldsymbol{x}) = -\alpha_{\rm bot}\, g(x, a_{\rm bot}, b_{\rm bot}, \sigma_{\rm bot}, \sigma_{\rm bot}).$$

with $\alpha_{\rm bot} = -3\,10^{-6}$, $a_{\rm bot} = b_{\rm bot} = 0.4\,L$, $\sigma_{\rm bot} = 0.04\,L$.

Initial data. The initial pressure considered in the simulation is given by (5.1). It is associated with the function $h = h(\boldsymbol{x})$ given by

$$h(\boldsymbol{x}) = \max\big\{0.9\, g(x,a,b,\sigma,\xi) - 3.35, h_{\rm bot} - 0.05\big\},$$

with $a = 0.3$, $b = 0.35$, $\sigma = 0.09$ and $\xi = 0.07$.

Geometry. The level of the bottom of the aquifer is defined for all $x \in \Omega_{2d}$ by

$$h_{\rm bot}(\boldsymbol{x}) = \sum_{k=1}^3 f_{\rm bot}^i(\boldsymbol{x}) - 5, \quad \text{with} \quad f_{\rm bot}^i(x,z) := \alpha_{\rm bot}^i\, g(x, c_x^i, d_x^i, \beta_x^i, \gamma_x^i),$$

and

$$\alpha_{\rm bot}^1 = 0.7, \quad c_x^1 = d_x^1 = 0.5\,L, \quad \beta_x^1 = 0.05\,L, \quad \gamma_x^1 = 0.2\,L,$$
$$\alpha_{\rm bot}^2 = 1, \quad c_x^2 = d_x^2 = 0.1\,L, \quad \beta_x^2 = 0.7\,L, \quad \gamma_x^2 = 0.2\,L,$$
$$\alpha_{\rm bot}^3 = 2, \quad c_x^3 = d_x^3 = L, \quad \beta_x^3 = 0.2\,L, \quad \gamma_x^3 = 0.1\,L.$$

A.2. Proof of Theorem 3.1 for the 3d-Richards model

The strategy of the proof is exactly the same as that followed in [23]. It consists of substituting the formal asymptotic expansion (3.18)–(3.21) into the rescaled 3d-Richards equations (3.10)–(3.13). A cascade of equations follows by identifying the powers of ε. Then we characterize the main order terms in the expansion (3.18). For simplicity, we suppress the superscript γ in the unknowns in this section.

General relations. First, we state the relations that do not depend on $\gamma \in \{0,1,2\}$. Substituting the asymptotic expansion (3.18) into the velocity equation (3.11), we obtain

$$\begin{cases} \overline{\boldsymbol{v}}_0 = -k_r(\overline{P}_0)\Big(\dfrac{1}{\rho g}\dfrac{\partial \overline{P}_0}{\partial \overline{z}} + 1\Big)\overline{\boldsymbol{K}}\boldsymbol{e}_3, & \text{in }]0,\overline{T}[\times\Omega \\ \overline{\boldsymbol{v}}_1 = -\dfrac{k_r(\overline{P}_0)}{\rho g}\overline{\boldsymbol{K}}\Big(\nabla_{\overline{x}}\overline{P}_0 + \dfrac{\partial \overline{P}_1}{\partial \overline{z}}\boldsymbol{e}_3\Big) - k_r'(\overline{P}_0)\,\overline{P}_1\Big(\dfrac{1}{\rho g}\dfrac{\partial \overline{P}_0}{\partial \overline{z}} + 1\Big)\overline{\boldsymbol{K}}\boldsymbol{e}_3 & \text{in }]0,\overline{T}[\times\Omega. \end{cases} \tag{A.8}$$

In the same way, we deduce from (3.12) that it holds in $]0,\overline{T}[$:

$$\begin{cases} \alpha\,\overline{P}_0+\beta\,\overline{\boldsymbol{v}}_0\cdot\boldsymbol{e}_3=\overline{f}_0^{\text{soil}}, \qquad \alpha\,\overline{P}_1+\beta\left(\overline{\boldsymbol{v}}_1\cdot\boldsymbol{e}_3-\overline{\boldsymbol{v}}_0\cdot\nabla_{\overline{x}}\overline{h}_{\text{soil}}\right)=\overline{f}_1^{\text{soil}}, \\ \alpha\left(\overline{P}_2+\dfrac{1}{2}\|\nabla_{\overline{x}}\overline{h}_{\text{soil}}\|^2\,\overline{P}_0\right)+\beta\left(\overline{\boldsymbol{v}}_2\cdot\boldsymbol{e}_3-\overline{\boldsymbol{v}}_1\cdot\nabla_{\overline{x}}\overline{h}_{\text{soil}}\right)=\dfrac{1}{2}\|\nabla_{\overline{x}}\overline{h}_{\text{soil}}\|^2\,\overline{f}_0^{\text{soil}}+\overline{f}_2^{\text{soil}} \end{cases} \tag{A.9}$$

on $\overline{\Gamma}_{\text{soil}}$;

$$\overline{\boldsymbol{v}}_0\cdot\boldsymbol{e}_3=\overline{f}_0^{\text{bot}}, \qquad \overline{\boldsymbol{v}}_{k-1}\cdot\nabla_{\overline{x}}\overline{h}_{\text{bot}}=\overline{\boldsymbol{v}}_k\cdot\boldsymbol{e}_3-\overline{f}_k^{\text{bot}} \qquad \text{on } \overline{\Gamma}_{\text{bot}}, \qquad \forall\, k\in\mathbb{N}^*; \tag{A.10}$$

$$\overline{\boldsymbol{v}}_k\cdot\overline{\boldsymbol{n}}=0 \qquad \text{on } \overline{\Gamma}_{\text{ver}}, \qquad \forall\, k\in\mathbb{N}^*. \tag{A.11}$$

Short time case. We consider $\gamma=0$ so that the time scale $T=\varepsilon^{-\gamma}\overline{T}$ corresponds to the case *short*. We prove the first claim of Theorem 3.1. Equation (3.10) reads

$$\phi\,\frac{\partial s(\overline{P})}{\partial\overline{t}}+\varepsilon\,\mathrm{div}_{\overline{\boldsymbol{x}}}(\overline{\boldsymbol{v}})+\frac{\partial\overline{\boldsymbol{v}}\cdot\boldsymbol{e}_3}{\partial\overline{z}}=\overline{f}. \tag{A.12}$$

The main order part of the last equation is

$$\phi\,\frac{\partial s(\overline{P}_0)}{\partial\overline{t}}+\frac{\partial\overline{\boldsymbol{v}}_0\cdot\boldsymbol{e}_3}{\partial\overline{z}}=\overline{f}_0 \qquad \text{in }]0,\overline{T}[\times\overline{\Omega}. \tag{A.13}$$

By combining this equation with the first equations in (A.8), (A.9) and (A.10), we obtain the system (3.22). This proves the first statement of Theorem 3.1.

Intermediate time case. We prove the second claim of Theorem 3.1. It is related to the intermediate time scale $T=\varepsilon^{-\gamma}\overline{T}$ for $\gamma=1$. Equation (3.10) is

$$\varepsilon\phi\,\frac{\partial s(\overline{P})}{\partial\overline{t}}+\varepsilon\,\mathrm{div}_{\overline{\boldsymbol{x}}}(\overline{\boldsymbol{v}})+\frac{\partial\overline{\boldsymbol{v}}\cdot\boldsymbol{e}_3}{\partial\overline{z}}=\overline{f}. \tag{A.14}$$

We substitute the asymptotic expansion (3.18) into the previous equation. By identifying the main order terms and considering the hypothesis (3.27), we derive

$$\frac{\partial\overline{\boldsymbol{v}}_0\cdot\boldsymbol{e}_3}{\partial\overline{z}}=\overline{f}_0=0 \qquad \text{on }]0,\overline{T}[\times\overline{\Omega}. \tag{A.15}$$

It follows that $\boldsymbol{v}_0\cdot\boldsymbol{e}_3$ is constant with respect to the variable $\overline{z}$. It is moreover zero due to (A.10) and (3.27). Because k_r and $\overline{K}_{zz}$ are non-vanishing ($\overline{\boldsymbol{K}}$ is positive definite), the first equation in (A.8) yields, in $]0,\overline{T}[\times\overline{\Omega}$,

$$\frac{\partial\overline{P}_0}{\partial\overline{z}}+\rho g=0 \qquad \text{and} \qquad \overline{\boldsymbol{v}}_0=0. \tag{A.16}$$

It follows the existence of $\overline{H}_0=\overline{H}_0(\overline{t},\overline{\boldsymbol{x}})$ with

$$\overline{P}_0(\overline{t},\overline{\boldsymbol{x}},\overline{z})=\rho g\big(\overline{H}_0(\overline{t},\overline{\boldsymbol{x}})-\overline{z}\big) \qquad \text{in }]0,\overline{T}[\times\overline{\Omega}. \tag{A.17}$$

This equation combined with (A.16)–(A.17), leads to (3.23). Subsequently, as $\overline{\boldsymbol{v}}_0 = 0$, the first equation in (A.9) is reduced to

$$\alpha\,\overline{P}_0 = \overline{f}_0^{\text{soil}} \qquad \text{on } \overline{\Gamma}_{\text{soil}}. \tag{A.18}$$

The rest of the proof depends on whether α is zero or not.

If $\alpha \neq 0$, we have $\overline{P}_0(\overline{t},\overline{\boldsymbol{x}},\overline{h}_{\text{soil}}(\overline{t},\overline{\boldsymbol{x}})) = \overline{f}_0^{\text{soil}}(\overline{t},\overline{\boldsymbol{x}})/\alpha$ in $]0,\overline{T}[\times\overline{\Omega_{2d}}$. Accordingly, by (A.17),

$$\overline{H}_0(\overline{t},\overline{\boldsymbol{x}}) = \frac{\overline{f}_0^{\text{soil}}(\overline{t},\overline{\boldsymbol{x}})}{\alpha\,\rho g} + \overline{h}_{\text{soil}}(\overline{t},\overline{\boldsymbol{x}}).$$

The second claim of Theorem 3.1 is proved if $\alpha \neq 0$.

If $\alpha = 0$ (then $\beta \neq 0$), Equation (A.18) implies the compatibility condition $\overline{f}_0^{\text{soil}} = 0$. We conclude the analysis by exploiting the next-order terms in the asymptotic expansion. We identify the coefficients associated with ε^1 in Equation (A.14) to obtain

$$\phi\,\frac{\partial s(\overline{P}_0)}{\partial\overline{t}} + \frac{\partial\overline{\boldsymbol{v}}_1\cdot\boldsymbol{e}_3}{\partial\overline{z}} = \overline{f}_1 \qquad \text{in }]0,\overline{T}[\times\overline{\Omega}. \tag{A.19}$$

We vertically integrate this equation on $]\overline{h}_{\text{bot}},\overline{h}_{\text{soil}}[$. It follows

$$\rho g\Big(\int_{\overline{h}_{\text{bot}}}^{\overline{h}_{\text{soil}}}\phi\,s'(\overline{P}_0)\,d\overline{z}\Big)\frac{\partial\overline{H}_0}{\partial\overline{t}} + (\overline{\boldsymbol{v}}_1|_{\overline{h}_{\text{soil}}} - \overline{\boldsymbol{v}}_1|_{\overline{h}_{\text{bot}}})\cdot\boldsymbol{e}_3 = \int_{\overline{h}_{\text{bot}}}^{\overline{h}_{\text{soil}}}\overline{f}_1\,dz, \tag{A.20}$$

where we have used (A.17) to write $\partial_{\overline{t}}(s(\overline{P}_0)) = \rho g s'(\overline{P}_0)\,\partial_{\overline{t}}\overline{H}_0$. Thanks to the second equations in (A.9) and (A.10) if $\alpha = 0$, and because $\overline{\boldsymbol{v}}_0 = 0$, we obtain

$$\overline{\boldsymbol{v}}_1\cdot\boldsymbol{e}_3 = \overline{f}_1^{\text{soil}}/\beta \quad \text{on } \overline{\Gamma}_{\text{soil}} \qquad \text{and} \qquad \overline{\boldsymbol{v}}_1\cdot\boldsymbol{e}_3 = \overline{f}_1^{\text{bot}} \quad \text{on } \overline{\Gamma}_{\text{bot}}. \tag{A.21}$$

Equation (A.20) thus takes the form

$$\rho g\Big(\int_{\overline{h}_{\text{bot}}}^{\overline{h}_{\text{soil}}}\phi\,s'(\overline{P}_0)\,d\overline{z}\Big)\frac{\partial\overline{H}_0}{\partial\overline{t}} = \int_{\overline{h}_{\text{bot}}}^{\overline{h}_{\text{soil}}}\overline{f}_1\,dz - \frac{\overline{f}_1^{\text{soil}}}{\beta} + \frac{\overline{f}_1^{\text{bot}}}{\beta}. \tag{A.22}$$

Equations (A.17) and (A.22) complete the proof of the second claim of Theorem 3.1 if $\alpha = 0$.

Long time case. We prove the third claim of Theorem 3.1. We consider $T = \varepsilon^{-\gamma}\overline{T}$ for $\gamma = 2$ corresponding to the long time scale. Equation (3.10) is

$$\varepsilon^2\phi\,\frac{\partial s(\overline{P})}{\partial\overline{t}} + \varepsilon\,\mathrm{div}_{\overline{\boldsymbol{x}}}(\overline{\boldsymbol{v}}) + \frac{\partial\overline{\boldsymbol{v}}\cdot\boldsymbol{e}_3}{\partial\overline{z}} = \overline{f}. \tag{A.23}$$

We substitute the asymptotic expansion (3.18) into the previous equation. The main-order part of the equation is $\partial_z(\overline{\boldsymbol{v}}_0\cdot\boldsymbol{e}_3) = \overline{f}_0 = 0$. As before, we obtain (3.23) for a function $\overline{H}_0$ that is constant on $\overline{z}$. It follows again (A.18) and also (3.24) if $\alpha \neq 0$.

On the other hand, if $\alpha = 0$, the compatibility condition $\overline{f}_0^{\text{soil}} = 0$ is imposed as before due to (A.18). We use the next-order part of Equation (A.23) to characterize $\overline{H}_0$. Thanks to (3.28) and the equality $\overline{\boldsymbol{v}}_0 = 0$, we get

$$0 = \overline{f}_1 = \operatorname{div}_{\overline{\boldsymbol{x}}}(\overline{\boldsymbol{v}}_0) + \frac{\partial \overline{\boldsymbol{v}}_1 \cdot \boldsymbol{e}_3}{\partial \overline{z}} = \frac{\partial \overline{\boldsymbol{v}}_1 \cdot \boldsymbol{e}_3}{\partial \overline{z}}. \tag{A.24}$$

Moreover, we use the second equations in (A.9) and (A.10) (for $k = 1$) to obtain (as $\alpha = 0$)

$$\beta\, \overline{\boldsymbol{v}}_1 \cdot \boldsymbol{e}_3 = \overline{f}_1^{\text{soil}} \quad \text{on } \overline{\Gamma}_{\text{soil}} \qquad \text{and} \qquad \overline{\boldsymbol{v}}_1 \cdot \boldsymbol{e}_3 = \overline{f}_1^{\text{bot}} = 0 \quad \text{on } \overline{\Gamma}_{\text{bot}}. \tag{A.25}$$

It follows that the vertically constant function $\overline{\boldsymbol{v}}_1 \cdot \boldsymbol{e}_3$ (due to (A.24)) is zero. The second compatibility condition $\overline{f}_1^{\text{soil}} = 0$ appears according to (A.25). Because $(\rho g)^{-1}\partial_{\overline{z}}\overline{P}_0 + 1 = 0$ and thanks to the second equation in (A.8), we obtain

$$\overline{\boldsymbol{v}}_1 = -\frac{k_r(\overline{P}_0)}{\rho g}\,\overline{\boldsymbol{K}}\Big(\nabla_{\overline{x}}\overline{P}_0 + \frac{\partial \overline{P}_1}{\partial \overline{z}}\,\boldsymbol{e}_3\Big).$$

As $\overline{\boldsymbol{v}}_1 \cdot \boldsymbol{e}_3 = 0$, it follows $\frac{\partial \overline{P}_1}{\partial \overline{z}} = -\frac{1}{\overline{K}_{zz}}\overline{\boldsymbol{K}}\nabla_{\overline{x}}\overline{P}_0 \cdot \boldsymbol{e}_3$, where K_{zz} in introduced in (2.3). We use equality $\overline{P}_0 = \rho g(\overline{H}_0 - \overline{z})$ in the last equation to obtain

$$\overline{\boldsymbol{v}}_1 = -k_r(\overline{P}_0)\,\overline{\boldsymbol{M}}\nabla_{\overline{x}}\overline{H}_0 \quad \text{with} \quad \overline{\boldsymbol{M}} = \begin{pmatrix} \mathbf{I}_2 & -\dfrac{\overline{\boldsymbol{K}}_{xz}}{\overline{K}_{zz}} \\ 0 & 0 \end{pmatrix}\overline{\boldsymbol{K}} = \begin{pmatrix} \overline{S}_0 & 0 \\ 0 & 0 \end{pmatrix} \tag{A.26}$$

where $\mathbf{I}_2$ is the 2×2 identity matrix and $\overline{S}_0 = \overline{\boldsymbol{K}}_{xx} - K_{zz}^{-1}\overline{\boldsymbol{K}}_{xz}\overline{\boldsymbol{K}}_{zx}$.

Because of Equation (A.11) for $k = 1$, we have $\overline{\boldsymbol{v}}_1 \cdot \overline{\boldsymbol{n}} = 0$ on $\overline{\Gamma}_{\text{ver}}$. The last equation in (3.26) is obtained as $k_r(\overline{P}_0)$ does not vanish. We identify the coefficients associated with ε^2 in Equation (A.23) to obtain

$$\phi\,\frac{\partial s(\overline{P}_0)}{\partial \overline{t}} + \operatorname{div}_{\overline{\boldsymbol{x}}}(\overline{\boldsymbol{v}}_1) + \frac{\partial \overline{\boldsymbol{v}}_2 \cdot \boldsymbol{e}_3}{\partial \overline{z}} = \overline{f}_2. \tag{A.27}$$

By (3.23), (A.26), and $\alpha = \overline{f}_0^{\text{bot}} = \overline{f}_1^{\text{bot}} = 0$, we can rewrite the third equation in (A.9) and the second equation in (A.10) for $k = 2$. We obtain

$$\overline{\boldsymbol{v}}_2 \cdot \boldsymbol{e}_3 - \overline{\boldsymbol{v}}_1 \cdot \nabla_{\overline{x}}\overline{h}_{\text{soil}} = \overline{f}_2^{\text{soil}}/\beta \qquad \text{on } \overline{\Gamma}_{\text{soil}}, \qquad \overline{\boldsymbol{v}}_2 \cdot \boldsymbol{e}_3 - \overline{\boldsymbol{v}}_1 \cdot \nabla_{\overline{x}}\overline{h}_{\text{bot}} = \overline{f}_2^{\text{bot}}/\beta \qquad \text{on } \overline{\Gamma}_{\text{bot}}. \tag{A.28}$$

We eliminate v_2 in system (A.27)–(A.28), by vertically integrating (A.27) on $[\overline{h}_{\text{bot}}, \overline{h}_{\text{soil}}]$. Thanks to the boundary conditions on $\overline{\Gamma}_{\text{bot}}$ and $\overline{\Gamma}_{\text{soil}}$, it follows

$$\begin{aligned} \frac{\partial}{\partial \overline{t}}\int_{\overline{h}_{\text{bot}}}^{\overline{h}_{\text{soil}}} \phi\, s(\overline{P}_0)\, d\overline{z} + \int_{\overline{h}_{\text{bot}}}^{\overline{h}_{\text{soil}}} \operatorname{div}_{\overline{\boldsymbol{x}}}\overline{\boldsymbol{v}}_1\, d\overline{z} + \overline{\boldsymbol{v}}_1|_{\overline{h}_{\text{soil}}} \cdot \nabla_{\overline{x}}\overline{h}_{\text{soil}} \\ + \frac{\overline{f}_2^{\text{soil}}}{\beta} - \overline{\boldsymbol{v}}_1|_{\overline{h}_{\text{bot}}} \cdot \nabla_{\overline{x}}\overline{h}_{\text{bot}} - \frac{\overline{f}_2^{\text{bot}}}{\beta} = \int_{\overline{h}_{\text{bot}}}^{\overline{h}_{\text{soil}}} \overline{f}_2\, dz. \end{aligned}$$

We use the Leibniz rule in the second integral to obtain

$$\frac{\partial}{\partial \overline{t}} \int_{\overline{h}_{\rm bot}}^{\overline{h}_{\rm soil}} \phi\, s(\overline{P}_0)\, d\overline{z} + \mathrm{div}_{\overline{\boldsymbol{x}}}\Big(\int_{\overline{h}_{\rm bot}}^{\overline{h}_{\rm soil}} \overline{\boldsymbol{v}}_1\, d\overline{z}\Big) = \int_{\overline{h}_{\rm bot}}^{\overline{h}_{\rm soil}} \overline{f}_2\, dz + \frac{\overline{f}_2^{\rm bot}}{\beta} - \frac{\overline{f}_2^{\rm soil}}{\beta}. \tag{A.29}$$

Thanks to the first equation in (A.26) and to the averaged conductivity $\overline{\boldsymbol{K}}$ defined in (3.2), we obtain

$$\int_{\overline{h}_{\rm bot}}^{\overline{h}_{\rm soil}} \overline{\boldsymbol{v}}_1\, d\overline{z} = -\int_{\overline{h}_{\rm bot}}^{\overline{h}_{\rm soil}} k_r(\overline{P}_0)\, \overline{\boldsymbol{M}} \nabla_{\overline{x}} \overline{H}_0\, d\overline{z} = -\overline{\boldsymbol{K}}(\overline{H}_0)\, \nabla_{\overline{x}} \overline{H}_0. \tag{A.30}$$

This equation combined with Equation (A.29) form the system (3.26). The proof of the last sentence of Theorem (3.1) is complete.

A.3. Proof of Theorem 3.1 for the *Fast-Slow* model

Short and intermediate timescales. The proofs for these cases are exactly the same as that done above for the 3d-Richards model. Indeed, by substituting the asymptotic expansion (3.18) into Equation (3.14) and by identifying the 0-order terms, we get the following relations holding in $]0, \overline{T}[\times\Omega$

$$\overline{\boldsymbol{v}}_0 = \overline{\boldsymbol{u}}_0 + \overline{\boldsymbol{w}}_0, \qquad \overline{\boldsymbol{u}}_0 = -k_r(\overline{P}_0)\, \overline{K}_{zz} \Big(\frac{1}{\rho g} \frac{\partial \overline{P}_0}{\partial \overline{z}} + 1 \Big) \boldsymbol{e}_3, \qquad \overline{\boldsymbol{w}}_0 = 0, \tag{A.31}$$

In particular,

$$\overline{\boldsymbol{v}}_0 = -k_r(\overline{P}_0)\, \overline{K}_{zz} \Big(\frac{1}{\rho g} \frac{\partial \overline{P}_0}{\partial \overline{z}} + 1 \Big) \boldsymbol{e}_3. \tag{A.32}$$

Moreover, Equations (A.9), (A.10) and (A.11) are still true and are derived as before from (3.12) which is also true for the model *Fast-Slow*. On the other hand, as (3.10) holds, we derive (A.12) for $\gamma = 0$ and (A.14) for $\gamma = 1$.

Equations (A.9), (A.10), (A.11), (A.12), (A.14) and (A.32) are the only ones that are used in the proof of Theorem (3.1) which is already done for the 3d-Richards model for the short and intermediate timescale. This proves the Theorem (3.1) for the coupled models in the cases of the short and intermediate timescales.

Long timescale. By substituting the asymptotic expansion (3.18) into Equation (3.14) and by identifying the 0 and 1-order terms, we get (A.32) and also the following relations holding in $]0, \overline{T}[\times\Omega$

$$\overline{\boldsymbol{v}}_1 = -\frac{k_r(\overline{P}_0)}{\rho g}\, \overline{K}_{zz} \Big(\frac{\partial \overline{P}_1}{\partial \overline{z}}\, \boldsymbol{e}_3 \Big) - k_r(\overline{P}_0)\, \overline{\boldsymbol{A}}(\overline{H}_0)\, \nabla_{\overline{x}} \overline{H}_0 - k_r'(\overline{P}_0)\, \overline{K}_{zz}\, \overline{P}_1 \Big(\frac{1}{\rho g} \frac{\partial \overline{P}_0}{\partial \overline{z}} + 1 \Big) \boldsymbol{e}_3. \tag{A.33}$$

Moreover, we deduce from (3.15) and (3.16) that

$$\overline{Q}_0(\overline{t}, \overline{x}, \overline{z}) = P_0(\overline{t}, \overline{x}, \overline{l}_0(\overline{t}, \overline{\boldsymbol{x}})) + \rho g \big(\overline{l}_0(\overline{t}, \overline{\boldsymbol{x}}) - \overline{z} \big), \tag{A.34}$$

$$\overline{H}_0(\overline{t}, \overline{\boldsymbol{x}}) = \frac{1}{\overline{l}_0(\overline{t}, \overline{\boldsymbol{x}}) - \overline{h}_{\rm bot}(\overline{\boldsymbol{x}})} \int_{\overline{h}_{\rm bot}(\overline{\boldsymbol{x}})}^{\overline{l}_0(\overline{t}, \overline{\boldsymbol{x}})} \frac{\overline{P}_0(\overline{t}, \overline{x}, \overline{z})}{\rho g} + \overline{z}\, d\overline{z}, \tag{A.35}$$

and from (3.17) that

$$\overline{l}_0(\overline{t},\overline{\boldsymbol{x}}) = \inf\left\{\overline{z}\in[\overline{h}_{\rm bot}(\overline{\boldsymbol{x}}),\overline{h}_{\rm soil}(\overline{\boldsymbol{x}})],\ \overline{P}_0(\overline{t},\overline{\boldsymbol{x}},\overline{z})\le P_{\rm sat}\right\} \qquad \text{for } (\overline{t},\overline{\boldsymbol{x}})\in[0,\overline{T}[\times\overline{\Omega_{2d}}. \tag{A.36}$$

We also obtain the same Equations (A.9), (A.10) and (A.11) from (3.12).

Moreover, we obtain Equation (A.23) from Equation (3.10). Identifying the main order terms from the asymptotic expansion gives (A.15). Since (A.10) hods true also in this case, we deduce (A.16), that is:

$$\frac{\partial\overline{P}_0}{\partial\overline{z}}+\rho g=0 \qquad \text{and} \qquad \overline{\boldsymbol{v}}_0=0.$$

Then, it exists a function $\overline{G}_0=\overline{G}_0(\overline{t},\overline{\boldsymbol{x}})$ independent on $\overline{z}$ such that $\overline{P}_0(\overline{t},\overline{\boldsymbol{x}},\overline{z})=\rho g\big(\overline{G}_0(\overline{t},\overline{\boldsymbol{x}})-\overline{z}\big)$ in $]0,\overline{T}[\times\overline{\Omega}$. By the second equation in (A.34), we obtain

$$\overline{H}_0(\overline{t},\overline{\boldsymbol{x}})=\frac{1}{\overline{l}_0(\overline{t},\overline{\boldsymbol{x}})-\overline{h}_{\rm bot}(\overline{\boldsymbol{x}})}\int_{\overline{h}_{\rm bot}(\overline{\boldsymbol{x}})}^{\overline{l}_0(\overline{t},\overline{\boldsymbol{x}})}\frac{\overline{P}_0(\overline{t},\overline{x},\overline{z})}{\rho g}+\overline{z}\,d\overline{z}=\overline{G}_0(\overline{t},\overline{\boldsymbol{x}}). \tag{A.37}$$

It follows that $\overline{P}_0(\overline{t},\overline{\boldsymbol{x}},\overline{z})=\rho g\big(\overline{H}_0(\overline{t},\overline{\boldsymbol{x}})-\overline{z}\big)$ in $]0,\overline{T}[\times\overline{\Omega}$, and, by using Equation (A.34),

$$\overline{Q}_0(\overline{t},\overline{x},\overline{z})=\overline{P}_0(\overline{t},\overline{x},\overline{l}_0(\overline{t},\overline{\boldsymbol{x}}))+\rho g\big(\overline{l}_0(\overline{t},\overline{\boldsymbol{x}})-\overline{z}\big)=\rho g\big(\overline{H}_0(\overline{t},\overline{\boldsymbol{x}})-\overline{z}\big)=\overline{P}_0(\overline{t},\overline{x},\overline{z}). \tag{A.38}$$

As in the proof associated with the 3d-Richards model, the characterization on $\overline{H}_0$ depends on the values of α. As before, we have (3.24) if $\alpha\neq 0$ and it remains to study the case $\alpha=0$. In this case, the compatibility condition $\overline{f}_0^{\rm soil}=0$ is also necessary because of (A.18). The identification of the next order term in Equation (A.23) yields (A.24). Then, thanks to (A.9) and (A.10) we obtain (A.25). Summarily:

$$\frac{\partial\overline{\boldsymbol{v}}_1\cdot\boldsymbol{e}_3}{\partial\overline{z}}=0 \quad \text{on } \Omega, \qquad \beta\,\overline{\boldsymbol{v}}_1\cdot\boldsymbol{e}_3=\overline{f}_1^{\rm soil} \quad \text{on } \overline{\Gamma}_{\rm soil} \qquad \text{and} \qquad \overline{\boldsymbol{v}}_1\cdot\boldsymbol{e}_3=0 \quad \text{on } \overline{\Gamma}_{\rm bot}.$$

The vertical component of $\overline{\boldsymbol{v}}_1\cdot\boldsymbol{e}_3$ then disappears and the compatibility condition $\overline{f}_1^{\rm soil}=0$ appears. Using Equation (A.33) and considering (A.38) and that $(\rho g)^{-1}\partial_{\overline{z}}\overline{P}_0+1=0$, we obtain

$$\overline{\boldsymbol{v}}_1=-\frac{k_r(\overline{P}_0)}{\rho g}\,\overline{K}_{zz}\Big(\frac{\partial\overline{P}_1}{\partial\overline{z}}\,\boldsymbol{e}_3\Big)-k_r(\overline{P}_0)\,\overline{\boldsymbol{A}}(\overline{H}_0)\,\nabla_{\overline{x}}\overline{H}_0.$$

As $\overline{\boldsymbol{v}}_1\cdot\boldsymbol{e}_3=0$ and $K_{zz}\neq 0$, we have $\partial_z\overline{P}_1=0$ and $\overline{\boldsymbol{v}}_1=-k_r(\overline{P}_0)\,\overline{\boldsymbol{A}}(\overline{H}_0)\,\nabla_{\overline{x}}\overline{H}_0$. In particular, and by (2.10), we find as before $\int_{h_{\rm bot}}^{h_{\rm soil}}\overline{\boldsymbol{v}}_1=-\overline{\boldsymbol{K}}(\overline{H}_0)\,\nabla_{\overline{x}}\overline{H}_0$, that is (A.30). The rest of the proof is exactly the same as that done above relatively to the 3d-Richards model. This concludes the proof of Theorem 3.1. □

REFERENCES

[1] R. Brooks and A. Corey, *Hydraulic Properties of Porous Media*. Colorado State University Hydrology Papers, Colorado State University, 1964.

[2] M. T. Van Genuchten, "A closed-form equation for predicting the hydraulic conductivity of unsaturated soils 1," *Soil science society of America journal*, vol. 44, no. 5, pp. 892–898, 1980.

[3] M. W. Farthing and F. L. Ogden, "Numerical solution of richards' equation: A review of advances and challenges," *Soil Science Society of America Journal*, vol. 81, no. 6, pp. 1257–1269, 2017.

[4] F. List and F. A. Radu, "A study on iterative methods for solving richards' equation," *Computational Geosciences*, vol. 20, pp. 341–353, mar 2016.

[5] I. Pop, F. Radu, and P. Knabner, "Mixed finite elements for the richards' equation: linearization procedure," *Journal of Computational and Applied Mathematics*, vol. 168, no. 1, pp. 365–373, 2004. Selected Papers from the Second International Conference on Advanced Computational Methods in Engineering (ACOMEN 2002).

[6] P. Forsyth, Y. Wu, and K. Pruess, "Robust numerical methods for saturated-unsaturated flow with dry initial conditions in heterogeneous media," *Advances in Water Resources*, vol. 18, no. 1, pp. 25–38, 1995.

[7] V. Casulli and P. Zanolli, "A nested newton-type algorithm for finite volume methods solving richards' equation in mixed form," *SIAM Journal on Scientific Computing*, vol. 32, no. 4, pp. 2255–2273, 2010.

[8] K. Brenner, "Acceleration of Newton's method using nonlinear Jacobi preconditioning," in *Finite volumes for complex applications IX—methods, theoretical aspects, examples—FVCA 9, Bergen, Norway, June 2020*, vol. 323 of *Springer Proc. Math. Stat.*, pp. 395–403, Springer, Cham, [2020] ©2020.

[9] K. Brenner and C. Cancès, "Improving newton's method performance by parametrization: The case of the richards equation," *SIAM Journal on Numerical Analysis*, vol. 55, no. 4, pp. 1760–1785, 2017.

[10] S. Bassetto, C. Cancès, G. Enchéry, and Q.-H. Tran, "On several numerical strategies to solve Richards' equation in heterogeneous media with finite volumes," *Comput. Geosci.*, vol. 26, no. 5, pp. 1297–1322, 2022.

[11] J. Dupuit, "Études théoriques et pratiques sur le mouvement des eaux dans les canaux découverts et à travers les terrains perméables," tech. rep., 1863.

[12] J. Bear, *Dynamics of Fluids in Porous Media*. New-York: Elsevier, 1972.

[13] J. Bear and A. Verruijt, *Modeling Groundwater Flow and Pollution*. Netherlands: Springer, 1987.

[14] G. Pantelis, "Saturated-unsaturated flow in unconfined aquifers," *Zeitschrift für angewandte Mathematik und Physik ZAMP*, vol. 36, pp. 648–657, Sep 1985.

[15] J. Kong, P. Xin, Z. yao Song, and L. Li, "A new model for coupling surface and subsurface water flows: With an application to a lagoon," *Journal of Hydrology*, vol. 390, no. 1, pp. 116 – 120, 2010.

[16] D. P. Viero, P. Peruzzo, L. Carniello, and A. Defina, "Integrated mathematical modeling of hydrological and hydrodynamic response to rainfall events in rural lowland catchments," *Water Resources Research*, vol. 50, no. 7, pp. 5941–5957, 2014.

[17] B. Jeannot, S. Weill, D. Eschbach, L. Schmitt, and F. Delay, "Assessing the effect of flood restoration on surface–subsurface interactions in rohrschollen island (upper rhine river – france) using integrated hydrological modeling and thermal infrared imaging," *Hydrology and Earth System Sciences*, vol. 23, no. 1, pp. 239–254, 2019.

[18] M. Chaguer, S. Weill, P. Ackerer, and F. Delay, "Implementation of subsurface transport processes in the low-dimensional integrated hydrological model nihm," *Journal of Hydrology*, vol. 609, p. 127696, 2022.

[19] M. F. Pikul, R. L. Street, and I. Remson, "A numerical model based on coupled one-dimensional Richards and Boussinesq equations," *Water Resources Research*, vol. 10, no. 2, pp. 295–302, 1974.

[20] M. Abbott, J. Bathurst, J. Cunge, P. O'connell, and J. Rasmussen, "An introduction to the european hydrological system - systeme hydrologique europeen,"SHE", 2: Structure of a physically-based, distributed modelling system," *Journal of Hydrology*, vol. 87, no. 1, pp. 61–77, 1986.

[21] A. Yakirevich, V. Borisov, and S. Sorek, "A quasi three-dimensional model for flow and transport in unsaturated and saturated zones: 1. implementation of the quasi two-dimensional case," *Advances in Water Resources*, vol. 21, no. 8, pp. 679 – 689, 1998.

[22] R. Paulus, B. J. Dewals, S. Erpicum, M. Pirotton, and P. Archambeau, "Innovative modelling of 3d unsaturated flow in porous media by coupling independent models for vertical and lateral flows," *Journal of Computational and Applied Mathematics*, vol. 246, pp. 38 – 51, 2013. Fifth International Conference on Advanced COmputational Methods in ENgineering (ACOMEN 2011).

[23] C. Bourel, C. Choquet, C. Rosier, and M. Tsegmid, "Modeling of shallow aquifers in interaction with overland water," *Appl. Math. Model.*, vol. 81, pp. 727–751, 2020.